Charles University
Faculty of Science

Study programme: Clinical and Toxicological Analysis

Branch of study: Clinical and Toxicological Analysis

Natália Remperová

Shape selectivity of ADOR zeolites in gas-phase m-xylene isomerisation

Bachelor's thesis

Supervisor:

Mgr. Michal Mazur, Ph.D.

Advisor:

Ing. Jan Přech, Ph.D.

Prague, 2021

Univerzita Karlova
Prírodovedecká fakulta

Študijný program: Klinická a toxikologická analýza

Študijný odbor: Klinická a toxikologická analýza

Natália Remperová

Tvarová selektivita zeolitov pripravených metódou ADOR v izomerizácii m-xylénu
v plynnej fáze

Bakalárska práca

Školiteľ:

Mgr. Michal Mazur, Ph.D.

Konzultant:

Ing. Jan Přech, Ph.D.

Praha, 2021

Prehlásenie

Prehlasujem, že som záverečnú prácu spracovala samostatne a že som uviedla všetky použité informačné zdroje a literatúru. Táto práca ani jej podstatná časť nebola predložená k získaniu iného alebo rovnakého akademického titulu.

V Prahe, 18. 6. 2021   Natália Remperová

Abstract

Zeolites are microporous crystalline aluminosilicates. They are used as catalysts due to their acidity, shape selectivity, high surface area, high thermal, and chemical stability. New types of zeolitic materials are of interests as catalysts for various reactions. Isomerisation of m-xylene is sensitive to shape and dimensionality of pores, thus it is excellent model reaction for zeolites characterisation.

The aim of this thesis is to investigate shape selectivity effects of isoreticular zeolites on the catalytic performance in m-xylene isomerisation. Isoreticular zeolites have the same crystalline layers connected in various way resulting in different, tuneable pore systems. The catalytic behaviour of the studied zeolites was compared to commercial ZSM-5 zeolite catalysts.

Isoreticular zeolites were prepared *via* ADOR method. This new method is a top-down approach for zeolite synthesis providing materials with preserved crystalline layers, but different channel systems. Parent Al-**UTL** (14- and 12-ring channels) zeolite was prepared *via* hydrothermal synthesis. This material was utilised for the synthesis of daughter zeolites with various channel systems: Al-IPC-7 (14- and 12-ring, as well as 12- and 10-ring channels), Al-IPC-2 (12- and 10-ring channels), Al-IPC-6 (12- and 10-ring, as well as 10- and 8-ring channels), and Al-IPC-4 (8- and 10-ring channels). The properties of prepared catalysts were characterised by powder X-ray diffraction, argon sorption, scanning and scanning transmission electron microscopy, and analysis of acid sites by infrared spectroscopy.

Isomerisation of m-xylene took place in a fixed-bed reactor at 350 °C. The highest conversion was provided by Al-IPC-7 catalyst with interconnected 14- and 12-ring channels, along with 12- and 10-ring channels, and also having the highest concentration of acid sites. In general, zeolites with 10-ring pores favoured monomolecular isomerisation thus providing a high p-xylene selectivity. Bimolecular reaction mechanism was enabled in 12- and 14-ring channels. The 8-ring channels were inaccessible, therefore their influence is neglectable. This caused practical decrease in the channel dimensionality to 1D pore system. Pore system controls selectivity and the presence of acid sites defines conversion with the presumption that the acid centres are accessible.

Key words: ADOR zeolites, shape selectivity, aluminium, catalysis, isomerisation, m-xylene, p-xylene

Abstrakt

Zeolity sú mikroporézne kryštalické aluminosilikáty. Uplatňujú sa ako katalyzátory, pretože sa vyznačujú kyslým charakterom, tvarovou selektivitou, veľkým povrchom, vysokou tepelnou a chemickou stabilitou. Nový druh materiálov je zaujímavé skúmať ako katalyzátory v rôznych rekciách. Izomerizácia m-xylénu je veľmi citlivá na tvar a dimenzionalitu pórov, je to teda výborná reakcia na charakterizáciu zeolitov.

Cieľom tejto práce bolo preskúmať vplyv tvarovej selektivity izoretikulárnych zeolitov na ich správanie sa v izomerizácii m-xylénu. Izoretikulárne zeolity pozostávajú z rovnakých kryštalických vrstiev, ktoré sú prepojené rôznymi spôsobmi a majú odlišné štruktúry pórov. Katalytické vlastnosti skúmaných zeolitov boli porovnané s komerčnými katalyzátoromi ZSM-5.

Izoretikulárne zeolity boli pripravené pomocou metódy ADOR. Táto nová metóda syntézy zeolitov poskytuje materiály so zachovanými kryštalickými vrstvami, no s odlišnými kanálovými systémami. Pôvodný Al-**UTL** zeolit (14- a 12-členné kanály) bol pripravený procesom hydrotermálnej syntézy. Tento materiál bol použitý na syntézu dcérskych zeolitov s rôznymi kanálovými systémami: Al-IPC-7 (14- a 12-členné, ako aj 12- a 10-členné kanály), Al-IPC-2 (12- a 10-členné kanály), Al-IPC-6 (12- a 10-členné, ako aj 10- a 8-členné kanály) a Al-IPC-4 (8- a 10-členné kanály). Vlastnosti pripravených katalyzátorov boli charakterizované práškovou röntgenovou difrakciou, sorpciou argónu, riadkovacím a riadkovacím transmisným elektrónovým mikroskopom a analýzou obsahu kyslých centier pomocou infračervenej spektroskopie.

Izomerizácia m-xylénu bola uskutočnená v reaktore s pevným lôžkom pri 350 °C. Najvyššia konverzia bola dosiahnutá pri použití katalyzátora Al-IPC-7 s prepojenými 14- a 12-člennými kanálmi spolu s 12- a 10-člennými kanálmi, a tiež s najvyššou koncentráciou kyslých centier. Pri použití zeolitov s 10-člennými kanálmi dochádzalo k uprednostneniu monomolekulárnej izomerizácie a k vysokej selektivite tvorby p-xylénu. Mechanizmus bimolekulárnej reakcie bol umožnený v 12- a 14-členných kanáloch. Vplyv 8-členných kanálov bol zanedbateľný, pretože boli neprístupné, čo prakticky zredukovalo pórový systém na 1D. Porézna štruktúra určuje selektivitu a prítomnosť kyslých centier, za predpokladu ich prístupnosti, definuje konverziu.

Kľúčové slová: ADOR zeolity, tvarová selektivita, hliník, katalýza, izomerizácia, m-xylén, p-xylén

Acknowledgement

Contents

List of abbreviations

ADOR	assembly-disassembly-organisation-reassembly
Al-**UTL**	three letter code given to specific structure by International Zeolite Association [1], structure with **UTL** topology containing framework aluminium
$A_{m\text{-}xylene}$	integrated area of the gas chromatography signal for m-xylene
BAS	Brønsted acid sites
BET	Brunauer-Emmett-Teller method for calculating surface areas
BJH	Barrett-Joyner-Halenda algorithm for calculating pore size distributions
DEDMS	diethoxydimethylsilane
D4R	double-four-rings
EDS	energy dispersive X-ray spectroscopy
FTIR	Fourier transform infrared spectroscopy
GC	gas chromatography
HPLC	high-performance liquid chromatography
ICP-MS	inductively coupled plasma mass spectrometry
IPC-1P	Institute-of-Physical-Chemistry Precursor [2]
IPC-2	Institute-of-Physical-Chemistry-2 type of material, zeolite having **OKO** topology [1]
IPC-4	Institute-of-Physical-Chemistry-4 type of material, zeolite having **PCR** topology [1]
IPC-6	Institute-of-Physical-Chemistry-6 type of material, zeolite having ***PCS** topology [1]
IPC-7	Institute-of-Physical-Chemistry-7 type of material [3]
LAS	Lewis acid sites

MFI	three letter structure code given to ZSM-5 type of material by International Zeolite Association [1]
NLDFT	non-local density functional theory
NMR	nuclear magnetic resonance
PXRD	powder X-ray diffraction
S	selectivity [%]
S_{BET}	specific surface area [$m^2 \cdot g^{-1}$]
SDA	structure directing agent
SEM	scanning electron microscopy
S_{EXT}	external surface area [$m^2 \cdot g^{-1}$]
STEM	scanning transmission electron microscopy
T-O-S	time-on-stream [min]
UTL	three letter code given to specific structure by International Zeolite Association [1]
V_{meso}	mesopore volume [$cm^3 \cdot g^{-1}$]
V_{mic}	micropore volume [$cm^3 \cdot g^{-1}$]
V_{tot}	total pore volume [$cm^3 \cdot g^{-1}$]
WHSV	weight hourly space velocity [h^{-1}]
X	conversion [%]
Y	yield [%]
ZSM-5	Zeolite Socony Mobil-5 type of material, zeolite with **MFI** topology [1]
ε (BAS)	molar absorption coefficient for Brønsted acid sites [$cm \cdot \mu mol^{-1}$]
ε (LAS)	molar absorption coefficient for Lewis acid sites [$cm \cdot \mu mol^{-1}$]
$\Sigma A_{i, norm}$	sum of areas of gas chromatography signals for all compounds normalised to the molar response of m-xylene

1   Introduction

Porous crystalline aluminosilicates, zeolites, are widely used as catalysts due to their acidity, shape selectivity, high surface area, high thermal and chemical stability, as well as non-toxicity. Conventional zeolites are three-dimensional (3D) solids usually prepared by solvothermal method. This approach is limited in control over the structure organisation and other properties of the final material [4, 5]. Recently discovered method for the zeolite synthesis, the ADOR approach, allows precise control of the synthesis and tuning the properties of produced materials. This alternative synthetic method enables preparation of structures build of the same 2D layers, but different interlayer connections – isoreticular zeolites [2]. As a result, it is possible to design and produce demanded pore systems, thus to prepare catalysts with the required properties.

Isomerisation of m-xylene is an important industrial process due to a high demand for p-xylene, which is a substrate for terephthalic acid production [6, 7]. This reaction is also suitable for zeolite characterisation as a standard test method [8, 9]. Two possible reaction pathways for m-xylene isomerisation are: monomolecular and bimolecular reaction mechanisms [6, 8, 9]. Zeolite acid sites catalyse reactions of both mechanisms [8]. In the most cases, the desired reaction pathway is monomolecular isomerisation because it provides o-xylene and high yields of p-xylene [8, 10]. Shape selectivity, achievable by the right choice of the catalyst, is a key to control the favoured reaction mechanism [10].

This work allows better understanding of the influence of the channel system and acidity of the family of isoreticular zeolites (Al-**UTL** and Al-IPC-n materials) on their performance in a catalytic reaction (isomerisation of m-xylene).

The aims of this bachelor project are:
- Synthesis of aluminium containing ADOR zeolites.
  - preparation of Al-**UTL** *via* traditional hydrothermal synthesis,
  - synthesis of isoreticular zeolites: Al-IPC-7, Al-IPC-2, Al-IPC-6, Al-IPC-4 with various pore structures using ADOR method,
  - preparation of Al-IPC-2 material using two synthetic procedures to tune the aluminium content in this material.
- Investigation of the structural and acidic properties of prepared materials.

- characterisation of: structure, crystallinity, and phase purity by powder X-ray diffraction; textural properties by argon sorption; crystal morphology by scanning electron microscopy; advanced structural characterisation, and interlayer distance investigation by scanning transmission electron microscopy,

- determination of the composition, focusing on the determination of aluminium content in samples by scanning transmission electron microscopy with energy dispersive spectroscopy and inductively coupled plasma mass spectrometry,

- analysis of acid sites by adsorption of acetonitrile followed by Fourier transform infrared spectroscopy.

- Comparison of catalytic performance of prepared isoreticular zeolites with commercial ZSM-5 catalyst in gas-phase isomerisation of m-xylene.

    - optimisation of the conditions of the catalytic process,

    - investigation of the shape selectivity effects to correlate them with the pore structure of catalysts,

    - description of the influence of acidity on the catalytic performance of materials.

2 Theoretical section

2.1 Zeolites

Aluminosilicate crystalline solids possessing microporous structure are highly interesting group of materials due to their extensive applications, mainly in catalysis, ion-exchange, and sorption. Zeolite framework consists of linked TO_4 tetrahedra [1, 4], (T stands for Si, Al, or other heteroatoms like Ge, Ti, B, *etc*.) [2]. When trivalent atom (*e.g.* Al^{3+}) is present in the structure, it generates formal negative charge that is compensated by cations. These extra-framework cations can be exchanged for proton generating Brønsted acid sites (BAS) [4, 11]. Generally, theoretical formula of aluminoscilicate zeolite is: $(M^+)_a(M^{2+})_b[Al_{(a+2b)}Si_{n-(a+2b)}O_{2n}] \cdot mH_2O$. The ratio of Si/Al is equal or higher than 1, which is known as the Löwenstein's rule [4]. Natural zeolites are hydrothermally developed minerals. The discovery of their exceptional properties led to the expansion of their synthetic preparation. Up to date, over 250 various structure types are recognised, and assigned with three-letter code by the Structural Commission of the International Zeolite Association [1].

Variability of the zeolitic frameworks provides diverse properties, such as high thermal and hydrothermal stability, shape selectivity, molecular sieving effect, and tuneable acidity [4, 12], and therefore they are utilised in many applications. Zeolites are used in catalytic cracking, alkylation reactions, as detergents and ion exchangers, in the water treatment, and for many other applications [13, 14]. Another benefit is their environmental asset, which lies not only in the replacement of dangerous substances, saving energy, and reducing the waste production in chemical processes, but also in direct environmental applications like wastewater purification or removal of toxic elements from polluted soils [7, 15].

2.1.1 Hydrothermal synthesis

R. M. Barrer in 1940s and R. Milton in 1950s reported the first modern-era method for zeolites preparation. At first, Si/Al ratio in the framework was limited to very low values (lower than 5) due to synthesis in entirely inorganic mixture. In 1961, tetramethylammonium hydroxide was introduced for the first time into the reaction mixture, which allowed to achieve higher Si/Al ratio (higher than 10). Thus, the addition

of organic quaternary ammonium compounds to the reaction mixture is considered to be an important breakthrough in the hydrothermal synthesis. Beta (the first high-silica zeolite) and ZSM-5, still important for contemporary applications, were prepared using quaternary ammonium cations few years later. Expansion of the synthetic procedures resulted in preparation of plenty of new zeolites with different frameworks and various pore sizes [4]. Zeolites are divided to four groups based on the number of tetrahedra forming their pore openings: small pore zeolites (8-ring openings), medium pore zeolites (10-ring openings), large pore zeolites (12-ring openings), and extra-large pore zeolites (14-ring and larger openings) [16]. Another division of zeolites is according to dimensionality of channels orientation: one-dimensional, two-dimensional (*e.g.* **UTL**) and three-dimensional (*e.g.* **MFI**) [1].

Hydrothermal synthesis is the most frequently used method for zeolites preparation utilising high temperature (80 – 250 °C) and autogenous pressure in a closed system (Teflon-lined stainless-steel autoclave) [4]. Temperature and pressure increase the reaction rate among complex ions and enhance the hydrolytic reaction [5]. Crystallisation time is another important parameter in the formation of zeolites, because it affects the induction period, nucleation, and crystal growth. Shorter time may result in amorphous material or not completed crystallinity. On the other hand, metastable nature of zeolites implies that too long crystallisation time can promote the formation of unwanted phases, such as low porosity zeolites or non-porous materials (*e.g.* quartz) [17].

Water plays many roles in the reaction mixture. It can be a solvent, be involved in the condensation reaction between silica and alumina, change the chemical and physical properties of reactants and product, enhance the reaction rate, or be a mineralizer [5]. Alkali hydroxides are used as mineralizing components, in some cases their cations have influence on the structure formation. Silicon and aluminium sources are taking part in the crystallisation of zeolitic framework, and their molar ratio in the reaction mixture has an impact on the final structure and its properties [5, 17].

Another substance, typically present in the reaction mixture, is an organic compound called structure directing agent (SDA), usually quaternary ammonium cation. Based on the SDA molecule, Si/Al ratio can be influenced. Presence of SDA molecules is one of the factors responsible for the crystallisation of the specific framework, so-called true templating. However, the use of some SDAs can produce more than one structure. Also, one structure can be prepared with different SDAs depending on the other synthesis

conditions [4, 17, 18]. Furthermore, stabilisation of zeolite framework is another function of SDAs [4].

Trivalent and tetravalent metal elements (Al, Ti, Ge, Ga, B, *etc.*) can be present in the zeolite structure [19]. Heteroatoms are able to change the properties of a zeolite catalyst, *e.g.* the incorporation of boron provides a weaker acidity of the material in comparison to aluminosilicates. Industrial TS-1 catalyst is created after introducing titanium into the **MFI** structure [4], which allowed to use it for selective oxidations. Use of various elements can also improve the synthetic procedures. Preparation of some zeolitic frameworks is problematic, however, it is possible to accomplish it by utilisation of heteroatoms. They can stabilise a crystallisation of particular secondary building units, important for the synthesis of desired framework. For example, creation of less stable three- and four-rings is feasible instead of preferred five- and six-ring openings. The example of such influence is the incorporation of germanium into the silicate or aluminosilicate that leads to the formation of double-four-ring (D4R) secondary building units after the crystallisation process (*e.g.* synthesis of **UTL** zeolite). It was shown, that the germanium presence can dominate the influence on structure formation over the SDA effect [2]. Germanosilicates are generally stable, however, under acidic conditions, the stability of Ge-O bonds is lower than Si-O bonds enabling controllable hydrolysis of GeO_4 tetrahedra. This feature was exploited in development of novel synthesis strategy called ADOR [2, 4]. This aspect is discussed in detail in Section 2.2. Complexity of the zeolite hydrothermal synthesis results in a limitation on the design and synthesis of new structures by this method [4, 5]. On the other hand, ADOR allows more precise control over the system than the standard hydrothermal approach, in some specific cases allowing preparation of energetically unfavourable zeolite topologies [2].

2.1.2   ZSM-5 zeolite

ZSM-5 (Zeolite Socony Mobil-5 [20]), firstly synthesised in 1965 by Landolt and Argauer, is among the most industrially important zeolites [21]. International Zeolite Association recognised it and assigned as the **MFI** framework type [1]. The structure consists of *mfi* units connected into pentasil chains, mirrored chains are linked *via* oxygen bridges resulting in 10-ring channels, creating 3D pore structure (Figure 2.1) [22], having characteristic zig-zag channels [23]. This material was found to have higher stability and was more slowly deactivated by coke than the zeolite Y, commercially used in cracking

[21]. Due to this traits, ZSM-5 catalyst was added to the industrial fluid catalytic cracking process [21]. Today, it is one of the most important industrially used zeolites [22]. ZSM-5 is utilised in acid catalysed reactions such as hydrocarbon alkylations, xylenes isomerisation, methanol-to-olefins conversion or methanol-to-gasoline process [7, 16, 22, 24]. ZSM-5 is also used for other, non-catalytic applications, such as organophilic adsorption, and as zeolite membranes in separation methods [25].

Possibility of preparation of ZSM-5 in many forms (*e.g.* 3D, pillared, layered, nanosponge), as well as with various framework metals (*e.g.* Ti, Sn) is a big advantage, since it enables adjusting the properties of a material for different applications. Titanosilicate **MFI** zeolite, TS-1, is used as a selective oxidation catalyst [22]. Zeolites can also be ion-exchanged with various metal cations to functionalise them for non-catalytic applications. For example, Cu-ZSM-5 is a part of optical sensors for oxygen detection at high temperatures [26].
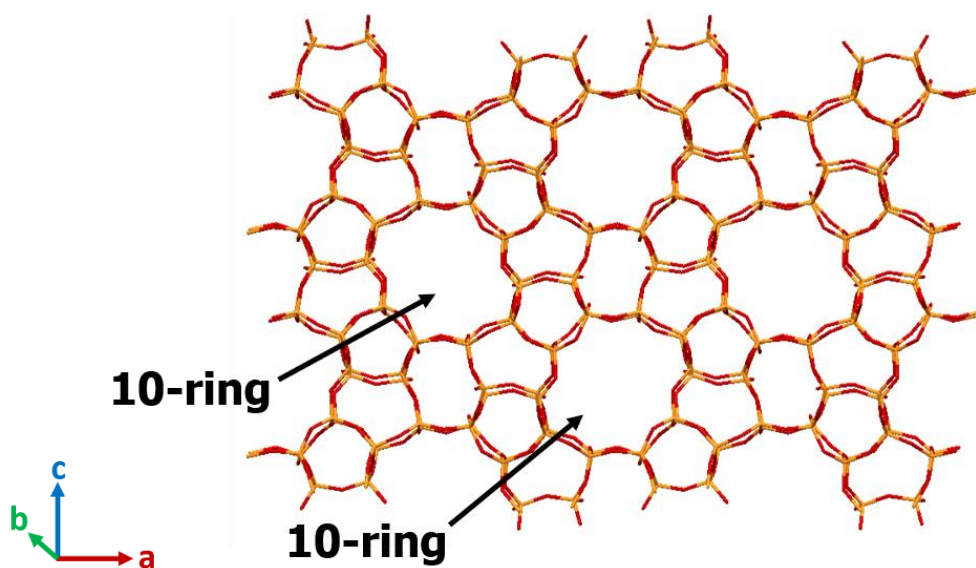
Figure 2.1 MFI structure showing 10-ring pores (view along [010]).

2.2   ADOR synthetic method

There are number of synthesis procedures that include the 2D zeolites. ADOR (Assembly-Disassembly-Organisation-Reassembly) approach for zeolite preparation (Figure 2.2) provides materials with preserved crystalline layers, but different channel systems [2]. It is a top-down strategy producing entirely connected 3D zeolites [13]. This novel strategy is based on controllable hydrolysis of parent 3D germanosilicate to produce a layered precursor. It is possible due to the architecture of parent zeolite [27], where

germanium is preferentially located in the double-four-ring units (D4R), between the silicate layers. Germanium is selectively removed from the interlayer positions during hydrolysis [13]. In the following step, it is possible to organise obtained layers in various ways. Ultimately, a new 3D zeolite can be produced after the reassembly step [2]. While germanium is preferentially located in D4Rs of parent zeolite, other elements (Si and Al) are mostly located in the layers, therefore vast majority of the acid sites important for catalysis remain in the structure of new 3D zeolite prepared by ADOR mechanism [13].

The first recognised parent ADOR-able germanosilicate was **UTL**. This zeolite has been used for preparation of IPC-1P, layered precursor of daughter IPC materials (IPC-2, IPC-4 [28], IPC-6, IPC7 [3], IPC-9 and IPC-10 [29]) produced by the ADOR method. Various trivalent metals can be introduced into the **UTL** structure (*e.g.* Al, B, Ga) providing different properties of the final material [19]. Isomorphous substitution of aluminium into the germanosilicate framework provides strong BAS [19]. **UTL** is not the only zeolite transformed using ADOR mechanism. SAZ-1 [30], **UOV** [31] and **IWW** [32] have also been used in ADOR synthetic process. Furthermore, **IWR** or **ITH** [33] zeolites are potential candidates.
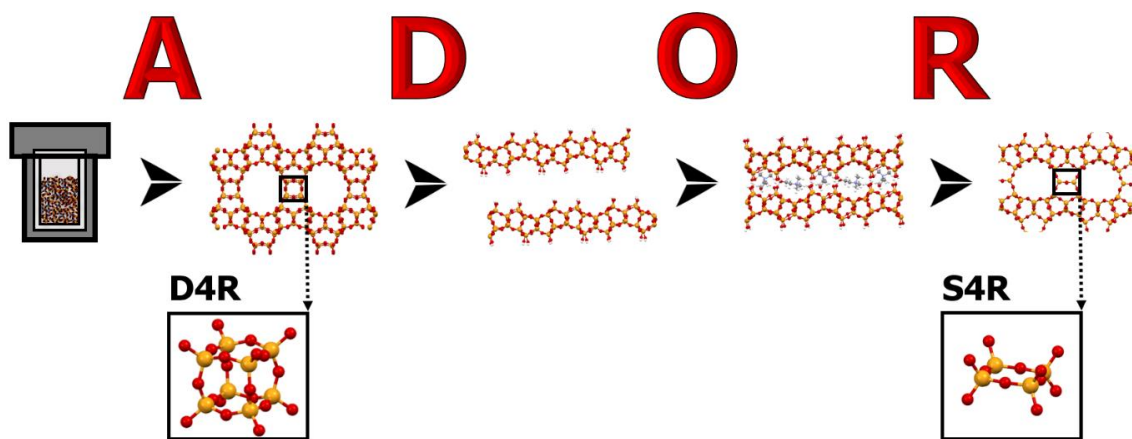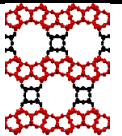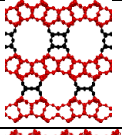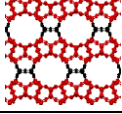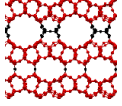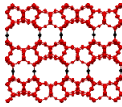
Figure 2.2 The scheme of ADOR method showing the four steps of the mechanism: A – assembly of a parent Al-**UTL** zeolite, D – disassembly to the layered precursor, O – organisation of layers, R – reassembly into new 3D IPC-2 (**OKO**) zeolite; D4R = double-four-ring, S4R = single-four-ring connecting units.

Germanosilicate **UTL** consists of the siliceous layers linked *via* double-four-ring units resulting in extra-large 12- and 14-ring pore zeolite (Table 2.1) [22]. Presence

of germanium, preferably in D4Rs connecting layers, enables selective removal of germanium to obtain undamaged layers. These characteristics are utilised in ADOR approach mentioned above. Presence of aluminium atoms in the **UTL** framework (*i.e.* Al-**UTL**) provides BAS important for catalytic reactions [27, 34].

Acidic hydrolysis of **UTL** generates a layered precursor IPC-1P [35]. Intercalation of organic amine in between the layers helps with their organisation, subsequent condensation of surface silanol groups leads to the formation of IPC-4 (**PCR**) zeolite. Layers in IPC-4 framework are connected *via* oxygen bridges resulting in 8- and 10-ring channel structure (Table 2.1) [2]. To prepare different zeolite from IPC-1P layeres, the ADOR steps are modified accordingly. Silylation using diethoxydimethylsilane in nitric acid solution leads to the formation of single-four-ring units between the layers. Zeolite obtained *via* silylation is called IPC-2 (**OKO**), this material has 12- and 10-ring channels (Table 2.1) [2]. IPC-2 zeolite can be also prepared using calcined Al-**UTL** in aluminium nitrate nonahydrate solution resulting in the material with higher aluminium content [36].

Table 2.1 Structural parameters of Al-**UTL** and Al-IPC zeolites.

Zeolite structure	Connecting unit[a]	Channel size [nm]						d-spacing [nm]
		14-ring	12-ring	12-ring	10-ring	10-ring	8-ring	
Al-**UTL**		0.95 x 0.71	0.85 x 0.55	–	–	–	–	1.44
Al-IPC-7		0.95 x 0.71	0.85 x 0.55	0.66 x 0.62	0.54 x 0.53	–	–	1.28
Al-IPC-2		–	–	0.66 x 0.62	0.54 x 0.53	–	–	1.14
Al-IPC-6		–	–	0.66 x 0.62	0.54 x 0.53	0.58 x 0.38	0.45 x 0.36	1.02
Al-IPC-4		–	–	–	–	0.58 x 0.38	0.45 x 0.36	0.91

[a] Connecting units: D4R = double-four-ring, S4R = single-four-ring, oxygen = oxygen bridge.

18

Furthermore, it is possible to prepare zeolites with two different types of interlayer connecting units in one zeolite. Combination of D4Rs and S4Rs is present in IPC-7 zeolite after two-step hydrolysis of calcined **UTL** in aluminium nitrate nonahydrate solution [3, 37]. As a result of combined connectivity, IPC-7 possesses two types of pore systems with 14- and 12-ring, as well as 12- and 10-ring channels (Table 2.1) [3, 37]. After tuning the hydrolysis and subsequent treatment conditions, IPC-6 (***PCS**) zeolite with S4R and oxygen connections is formed [37]. Due to the existence of S4Rs and oxygen bridges, two forms of connectivity with 12- and 10-ring, along with 10- and 8-ring channels are present in IPC-6 material (Table 2.1) [3, 37]. IPC-7 and IPC-6 are indicated as disordered materials due to the non-perfect alteration of the layer-connecting units [3].

To conclude, the D4R units from parent **UTL** zeolite can be replaced in four ways: 1) by combination of D4Rs and S4Rs (IPC-7); 2) by S4Rs (IPC-2); 3) by combination of S4Rs and oxygen bridges (IPC-6); 4) exclusively by oxygen bridges (IPC-4) (Table 2.1). These isoreticular zeolites differ in the channel sizes and interlayer connections, but the crystalline layers are the same. Thus, this zeolite family is suitable model system for shape-selectivity studies in catalytic gas-phase m-xylene isomerisation [3, 37].

2.3   Applications of zeolites in catalysis

Zeolites are typical materials used in heterogenous catalysis where the catalyst is in a different phase than reactants and products [7]. Their exceptional properties such as thermal stability, reusability, separability, variability in pore systems and composition, shape selectivity, tuneable acidity, and non-toxicity makes them intensively applied in oil refining and petrochemistry [38, 39]. Toxic homogeneous catalysts (*e.g.* sulphuric acid, hydrofluoric acid) have been replaced by zeolites which brought the environmental and economic profits [27, 39, 40].

Acidic character of aluminosilicates is crucial for their use in catalysis [27]. Zeolites can possess both Brønsted and Lewis acid sites. When trivalent atoms (*e.g.* Al^{3+}) are present in the framework, resulting AlO_4^- tetrahedra are negatively charged. Protons compensate negative charges in the framework creating Brønsted acid sites (BAS) [27, 34, 41]. Brønsted acid is a proton donor, that transfers a proton to the acceptor [11]. Framework substitution of heteroatoms, extra-framework trivalent aluminium atoms (Al^{3+}) and extra-framework cations for charge compensation provide also Lewis acid centres (LAS) in zeolites, acceptors of the electron pairs [42]. The zeolite structure or

chemical composition can be also modified post-synthesis, which can influence the concentration and strength of zeolite acid sites [27].

All described features of zeolites place them among the most important heterogenous catalysts. Fluid catalytic cracking, hydrocracking, selective catalytic reduction of nitrogen oxides, hydroisomerisation, and catalytic dewaxing are very important processes catalysed by zeolites [7, 27, 38, 43]. Among the most significant petrochemical processes is xylene isomerisation (aiming to produce particularly p-xylene) and other processing of aromatics (alkylation, transalkylation and disproportionation) [7, 8, 27, 38, 44]. Zeolites are also used to produce fine chemicals [7, 27].

2.3.1   Isomerisation of m-xylene

Isomerisation of m-xylene in an important petrochemical process due to selectivity towards p-xylene production [6, 7]. P-xylene is the most valuable xylene isomer because of its use in the terephthalic acid and dimethyl terephthalate conversion to polyethylene terephthalate (PET). Subsequently, it allows preparation of synthetic fibres and plastics [7, 45]. Isomerisation of m-xylene can also serve as a model reaction for characterisation of the zeolite properties [8, 9]. Geometry and architecture of channel system, framework composition, and its influence on activity and selectivity can be investigated by performing xylene isomerisation [9].

Xylene isomerisation can proceed *via* two possible pathways, monomolecular and bimolecular mechanisms (Figure 2.3) [6, 8, 9]. The parameter determining the preferred reaction mechanism is the reaction space [10]. Monomolecular isomerisation is favoured in 10-ring zeolites giving o-xylene and high yield of p-xylene [8, 10]. Bimolecular disproportionation is dominant in case of 12-ring channels. They allow the formation of transition state resulting in the production of trimethylbenzenes and toluene [8, 10, 46]. One of the drawbacks is a fact that during the reaction, the coke is formed in zeolite pores, causing the deactivation of it. Coking of 10-ring zeolites is slower than 12-ring zeolites [46]. Toluene disproportionation may occur when the reaction follows the bimolecular mechanism of xylene isomerisation, and therefore, benzene and xylene can be formed [8].

Monomolecular isomerisation of xylenes is preferred reaction mechanism over medium-pore ZSM-5 and gives high p-xylene selectivity due to product-shape selectivity [8, 10]. Steric hindrances provided by 10-ring pores do not allow the formation

of transition state required for bimolecular reaction mechanism [9]. It was shown that the architecture, zeolite pores dimensionality, and their arrangement are influencing factors on the m-xylene isomerisation mechanism [9].

Isomerisation
(monomolecular)

a	Primary reaction	Confinement preferred	Fast
b	Primary reaction	Confinement preferred	Fast

Dispropotionation
(bimolecular)

c	Primary reaction	Confinement suppressed	Fast
d	Secondary reaction	Confinement preferred	Slow
e	Secondary reaction	Confinement suppressed	Slow
f	Secondary reaction	Confinement suppressed	Slow
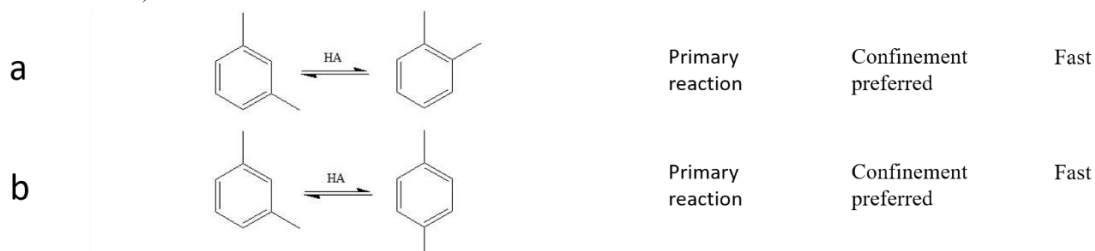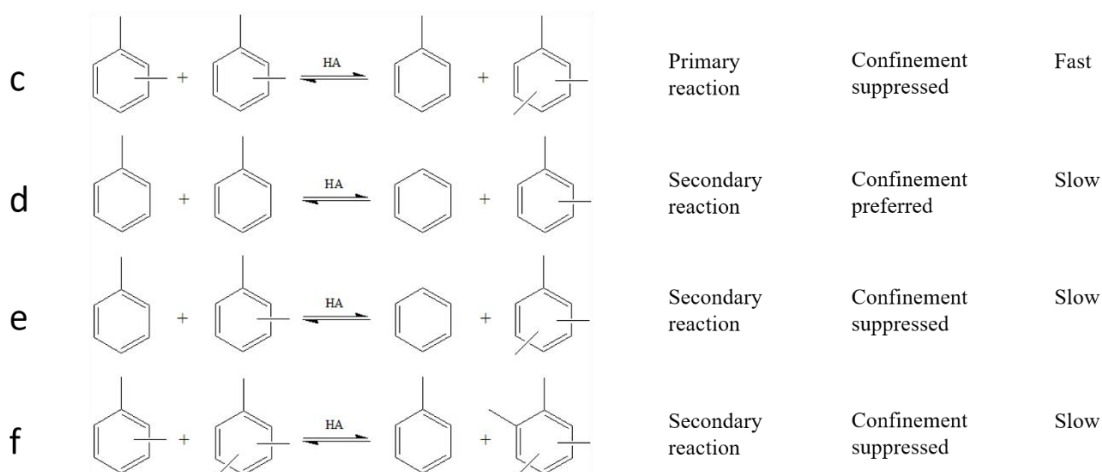
Figure 2.3 Simplified reaction scheme of possible reaction pathways in m-xylene isomerisation reaction showing (a, b) monomolecular reaction mechanism and (c – f) bimolecular reaction mechanism.

2.4   Characterisation methods for zeolitic materials

2.4.1   Methods used for characterisation of materials

Powder X-ray diffraction

The most common technique for determination of a zeolite structure is powder X-ray diffraction (PXRD). Zeolites are crystalline materials mostly prepared in a powder form, therefore PXRD is used for characterisation of their structure. A single-crystal X-ray diffraction, which enables to study the structure of large crystals, is rarely used for zeolite

21

characterisation, because it is usually not possible to synthesise sufficiently big single crystal of a zeolite. The principle of PXRD lies in the interaction of electromagnetic waves, X-rays, with a sample. Incoming X-rays are scattered by electrons in atoms, if these emitted waves satisfy Bragg equation (2.1) constructive interference occurs and XRD peaks are produced [47]. Diffracted radiation recorded by the detector gives information about electron density and based on that about structure. Diffraction occurs only at certain angles which satisfy Bragg equation (2.1), where d is perpendicular distance between the two plains, θ is the angle between the incident radiation and the lattice planes, n is an integer value and λ is the wavelength of incident radiation [48].

$$2d\sin\theta = n\lambda \tag{2.1}$$

Diffraction pattern is created based on diffraction spots of many properly oriented small crystals which satisfy Bragg equation (2.1). The structure is identified based on comparison with known diffraction patterns from database [22, 47].

Scanning electron microscopy

The crystals morphology of prepared catalysts can be characterised by scanning electron microscope [49]. It is possible to analyse samples with micro- or even nano-meter resolution. Primary electrons which are focused thanks to electromagnetic lenses scan the surface of the sample. Electrons interact with the specimen, what results in backscattered electrons (elastic scattering) or secondary electrons (inelastic scattering). Detection of these electrons provides information about morphology, size, and size ditribution of particles (if present) of catalyst crystals.

Scanning transmission electron microscopy

Scanning transmission electron microscopy is a method which combines moving of the focused electron beam and transmission technique to achieve higher (atomic) resolution [49]. This method gives information about structure of catalyst, *e.g.* to observe zeolite layers and pore systems.

The elemental analysis of sample is possible after combination of STEM with energy dispersive X-ray spectroscopy [49]. After the interaction of the electron beam with the sample, the X-rays with specific energy are emitted. The detection of them gives information about each element in the crystal allowing generation of elemental distribution maps.

Gas adsorption

Textural properties: pore volume and surface area, can be determined by gas adsorption. Gas (*e.g.* nitrogen, argon) is physisorbed (reversible weak adsorption) on the surface of a solid material [17, 47]. Adsorption isotherm is obtained as a result of adsorption at constant temperature lower than the critical temperature of the adsorbate. It describes the relation between partial pressure and the amount of adsorbed gas. The amount of adsorbed gas depends on the temperature, pressure, and type of the adsorbate [47, 50]. Nitrogen and argon are the most frequently used gases for adsorption. However, nitrogen is not always suitable due to its specific interactions with surface of adsorbent [50]. The temperature of nitrogen and argon adsorption are -196.15 °C and -186.15 °C, respectively [47, 50]. Surface area of a material is calculated by the Brunauer-Emmett-Teller method [51, 52]. This method is founded on Langmuir theory and additionally includes multilayer adsorption of gas [47]. For the calculation of mesopore volume and size distribution is often used Barrett-Joyner-Halenda algorithm [51, 53]. Information about micropore volume and pore size distribution can be obtained using non-local density functional theory [50, 54].

Inductively coupled plasma mass spectrometry

The presence and concentration of heteroatoms in a zeolite are very influential features when it comes to utilisation of these materials. Inductively coupled plasma mass spectrometry (ICP-MS) is a method for analysis of the elemental composition of a sample [55]. The advantages of this technique are ionisation in chemically inert environment, self-absorption decrease and a wide linear range for calibration. Samples, usually in a liquid phase, are nebulised and resulting aerosol is atomised in plasma at approx. 6 000 °C inside the torch. Then, atoms are ionised and migrate to the interface which consists of a sampler cone and a skimmer cone (the place where ICP part and MS part are connected). In this part, two-step pressure reduction happens.

After focusing, ions enter the quadrupole of the mass spectrometer and are separated. Ions are analysed according to their mass-to-charge ratio [55]. Resulting mass spectrum (a plot of an intensity as a function of the mass-to-charge ratio) is characteristic for detected compound [56]. ICP-MS is very sensitive method with detection limits at ppb, and in some cases even at ppt level [57].

Fourier transform infrared spectroscopy

Zeolite acidity plays a crucial role in catalytic reactions. The most used technique for determination of acid sites in zeolite catalysts is infrared spectroscopy [42]. Concentration of acid sites is determined by adsorption of basic probe molecules (*e.g.* pyridine, ammonia, carbon monoxide, acetonitrile) on them [58]. Infrared spectroscopy is able to identify functional groups of the molecules. Vibrational excitations of molecules caused by a change of a dipole moment are fundamental principles of infrared spectroscopy. Vibration frequency depends on the type of the atom or group and also on weak interactions with the surrounding environment [58]. The FTIR spectrum is obtained after the Fourier transformation of the interferogram. It is possible to differentiate between Brønsted and Lewis acid sites based on different interaction with basic molecules [59]. Although the most used probe molecule is pyridine, it is not suitable for narrower than 10-ring pores due to size restrictions. Acetonitrile is used as a probe molecule for smaller pores [59].

2.4.2 Methods for the analysis of the synthesis precursors and evaluation of the catalytic experiments.

Nuclear magnetic resonance spectroscopy

Some organic structure directing agents (SDAs) for zeolite preparation are not commercially available. Thus, it is necessary to synthesise them from available substrates. Nuclear magnetic resonance is utilised for the confirmation of structure and purity of synthesised organic compounds [60]. This method is based on the fact that atoms having nuclei with non-zero magnetic moments (*e.g.* ^{1}H) are interacting with external magnetic field. Stationary states of nuclei are stimulated by a radiofrequency pulse and the absorbed energy is detected, which results in resonance signal. The chemical surrounding of the nucleus can be determined due to different types and numbers of bonds characterising each nucleus. In this way, we are able to confirm the structure of synthesised organic SDA, a crucial factor for the preparation of desired zeolite.

Gas chromatography

To analyse the performance of the catalyst, the samples of the reaction mixture are collected in different times to analyse its composition. The investigation is realised by gas chromatography. It is a method for separation and analysis of organic compounds.

Vaporised mixture of compounds transported by a carrier gas (*e.g.* helium, nitrogen) is separated in a column, then individual compounds are detected. For various molecules it takes a different time to travel through the column, based on the interaction with the stationary and mobile phase (carrier gas). This results in the separation of the components of the mixture. The carrier gas is required to be inert and cannot interact with the stationary phase [61]. The components of the mixture are retarded by the stationary phase based on their interaction with it. Composition of stationary phase can be modified depending on the analysed mixture [61, 62]. Then, separated ingredients of the reaction mixture are analysed. Among the possible detectors, flame ionisation detector (FID), a mass-sensitive detector, is commonly used due to its unique properties. Linear operating range, low price, speed of response, or unit carbon response (is not dependent on compound structure), *etc.* are the reasons for its frequent utilisation. FID detects ions generated after the combustion of the sample in hydrogen flame, and therefore is suitable for most hydrocarbons [63].

3 Experimental part

3.1 List of used chemicals

Commercially available chemicals which were used for zeolite preparation and following characterisation are listed in Table 3.1.

Table 3.1 List of used chemicals

Chemical	Purity	Manufacturer
1,5-dibromopentane	97%	Sigma-Aldrich
2-ethylpiperidine	>98%	TCI
Acetic acid	100%	Supelco
Acetonitrile	≥99.9%	Sigma-Aldrich
Acetonitrile-d_3	99.96%	Sigma-Aldrich
Aluminium hydroxide	≥63.5%	Acros Organics
Aluminium nitrate nonahydrate	≥98%	Sigma-Aldrich
Ambersep 900(OH)	–	Alfa Aesar
Carborundum 0.500 mm	–	VWR
Chloroform D1	99.8%	Carl Roth
Diethylether	100%.	VWR
Diethoxydimethylsilane	97%	Sigma-Aldrich
Ethanol absolute	>99.8%	Penta
Germanium oxide	≥99.9%	Sigma-Aldrich
Hydrofluoric acid	47 – 51%	ANALPURE®
Hydrochloric acid	34 – 37%	ANALPURE®
Nitric acid	67 – 69%	ANALPURE®
Nitric acid	65% G.R.	Lachner
m-Xylene	99%	Alfa Aesar
Octylamine	≥99%	Sigma-Aldrich
Orthoboric acid	≥99.8%	VWR
Potassium carbonate	≥99% P.A.	Fluka
Silica, fumed	–	Sigma-Aldrich

3.2   Synthesis of SDA

The organic compound, 1-ethyl-6-azoniaspiro[5.5]undecane hydroxide, was used for the synthesis of Al-**UTL** zeolite as SDA.

At first, 1,5-dibromopentane (1 eq), potassium carbonate (1.2 eq) and acetonitrile (250 ml) were mixed together and then, 2-ethylpiperidine (1 eq) was added dropwise in over 30 min. The reaction mixture was heated under reflux at 85 °C for 20 h. Acetonitrile was evaporated on a rotary evaporator and the product was dissolved in ethanol. The insoluble compounds were subsequently filtered out and washed with ethanol. The liquid was evaporated to almost saturated solution. Afterwards the solid was dissolved in the smallest possible amount of ethanol and diethylether was added to precipitate the product. The white product was separated by filtration and washed with ethanol. The organic SDA was dried in a hood for 24 h and then at 60 °C in a dryer for 12 h. The yield of the product was 72 %. The structure and purity of the synthesised SDA were confirmed with ^{1}H NMR spectroscopy.

After the synthesis of 1-ethyl-6-azoniaspiro[5.5]undecane bromide, ion exchange was proceed to obtain required organic compound. Prior to the ion exchange, resin was washed with distilled water (1 g of resin/10 ml of distilled water). 1-ethyl-6-azoniaspiro[5.5]undecane bromide, washed resin and distilled water (1 g of SDA/6.35 g of resin/5.15 g of distilled water) were mixed at room temperature for 16 h and then filtered. The solution was exchanged again with new washed resin, the process was repeated at the same conditions using the same reagent ratio. The resulting solution was used to synthesise Al-**UTL**.

3.3   Synthesis of ADOR zeolites

3.3.1   Al-**UTL**

Aluminium containing germanosilicate was prepared using 1-ethyl6-azoniaspiro[5.5]undecane hydroxide as SDA. Aluminium hydroxide was dissolved first in the aqueous SDA solution and then germanium dioxide was added. Finally, silica was added and the mixture was stirred at room temperature for 40 min. The final molar composition of the gel was 0.788 SiO_2/0.4 GeO_2/0.012 $AlO_{1,5}$/0.4 SDA/30 H_2O, pH was adjusted with hydrochloric acid to 12. The 100ml Teflon-lined stainless-steel autoclaves containing the resulting mixture were heated to 175 °C

for 28 days with tumbling (50 rpm). The solid product was filtered, washed with distilled water and dried at 60 °C for 12 h. The synthesised zeolite was calcined in a flow of air at 550 °C (a temperature ramp of 3 °C · min^{-1}) for 10 h.

3.3.2   Al-IPC-1P

Calcined Al-**UTL** was stirred with 1M acetic acid solution (1g of Al-**UTL**/1l of CH$_3$COOH) at 75 °C for 16 h. The product, Al-IPC-1P, was separated by filtration, washed with distilled water and dried at 60 °C for 12 h.

3.3.3   Al-IPC-7

Al-IPC-7 zeolite was synthesised in two steps. The first step was to hydrolyse calcined Al-**UTL** with 3M aluminium nitrate nonahydrate (1 g of Al-**UTL**/100 ml of Al(NO$_3$)$_3$ · 9H$_2$O) at 80 °C for 2 h. The white solid was separated by filtration and dried at 60 °C for 12 h. The second step of the preparation was again hydrolysis: the solid product was stirred with 1M aluminium nitrate nonahydrate (1 g of Al-**UTL**/100 ml of Al(NO$_3$)$_3$ · 9H$_2$O) at 80 °C for 2 h. The resulting product was isolated by filtration, dried at 60 °C for 12 h and subsequently calcined at 550 °C (a temperature ramp of 2 °C · min^{-1}) for 6 h.

3.3.4   Al-IPC-2

Materials having the IPC-2 framework were prepared by two synthetic strategies:

ADOR stepwise preparation
To synthesise the Al-IPC-2 ADOR, IPC-1P was mixed with 1M nitric acid solution and diethoxydimethylsilane (1 g of IPC-1P/10 g of HNO$_3$/0.5 g of DEDMS). The reaction was performed in the Teflon-lined stainless-steel autoclave at 175 °C for 16 h under tumbling conditions (50 rpm). The solid product was filtered, washed with distilled water, dried at 60 °C for 12 h and calcined in a flow of air at 550 °C (a temperature ramp of 2 °C · min^{-1}) for 10 h.

One-pot transformation of Al-UTL to Al-IPC-2
Al-IPC-2 one-pot was prepared using calcined Al-**UTL** mixed with 3M aluminium nitrate nonahydrate (1 g of Al-**UTL**/100 ml of Al(NO$_3$)$_3$ · 9H$_2$O). The reaction mixture was

heated under reflux at 80 °C for 2 h. The white product was filtered, washed with distilled water and dried at 60 °C for 12 h. The prepared zeolite was calcined in a flow of air at 550 °C (a temperature ramp of 2 °C · min^{-1}) for 10 h.

3.3.5   Al-IPC-6

Al-IPC-6 zeolite was synthesised in two steps. The first step was hydrolysis of calcined Al-**UTL** with 1M acetic acid and 1.6M aluminium nitrate nonahydrate (1 g of Al-**UTL**/150 ml of CH_3COOH/100 ml of $Al(NO_3)_3 \cdot 9H_2O$) at 85 °C for 16 h. The white solid was separated by filtration, washed with distilled water and dried at 60 °C for 12 h. The second step of the preparation was intercalation of octylamine. The solid product was stirred with octylamine (1 g of zeolite/13 g of octylamine) at 60 °C for 16 h. The resulting product was separated by centrifugation (3000 rpm for 10 min), two times centrifuged with distilled water, dried at 60 °C for 12 h and calcined at 650 °C (a temperature ramp of 3 °C · min^{-1}) for 10 h.

3.3.6   Al-IPC-4

To obtain Al-IPC-4 zeolite, intercalation of organic amine was performed. The mixture of 1 g of IPC-1P and 65 g of octylamine was heated under reflux at 70 °C for 4 h under stirring conditions. The solid product was isolated by centrifugation (3000 rpm for 10 min), two times washed with distilled water and dried at 60 °C for 12 h. The synthesised zeolite was calcined in a flow of air at 550 °C (a temperature ramp of 2 °C · min^{-1}) for 10 h.

3.4   Characterisation methods

3.4.1   Nuclear magnetic resonance

The structure of prepared SDAs was confirmed using a Bruker Ascend 400 MHz NMR spectrometer to record ^{1}H NMR spectra. The solvent used was chloroform D1.

3.4.2   Powder X-ray diffraction

The crystalline structure of the synthesised materials was determined by powder X-ray diffraction measurement using a Bruker AXS D8 Advance diffractometer equipped with a graphite monochromator and a position sensitive detector LYNXEYE XE-T using

Cu K_α radiation in Bragg-Brentano geometry. The sample holder was rotated during the data collection, the range of angles was 3 – 40 ° and the collection time was 25 min.

3.4.3   Argon sorption

A Micromeritics 3Flex volumetric Surface Area Analyzer at –186 °C was used to obtain adsorption isotherms of argon for determination of surface area, pore volume and pore size distribution. Prior to the measurement, samples were degassed under the turbomolecular pump vacuum starting at an ambient temperature up to 110 °C (a temperature ramp of 1 °C · min^{-1}) until the residual pressure of 13.3 Pa was achieved using a Micromeritics Smart Vac Prep instrument. After further heating at 110 °C for 1 h, the temperature was increased to 250 °C (1 °C · min^{-1}) and maintained for 8 h.

The BET method [51, 52] using adsorption data in the range of a relative pressure $p/p_0 = 0.05 – 0.20$ was used to evaluate the specific surface area. The external surface area was calculated by the t-plot method [51, 64]. The total adsorption capacity is represented by the adsorbed amount at relative pressure $p/p_0 = 0.95$. The mesopore volume and mesopore size distributions in the range 5 – 20 nm were calculated using the BJH algorithm [51, 53] from the desorption branch of the isotherms. To estimate the micropore volume and the pore size distributions Non-Local Density Functional Theory [54] using standard Micromeritics software for cylindrical pores (argon on oxides at –186 °C) was applied.

3.4.4   Fourier transform infrared spectroscopy

Prior to the FTIR study, the self-supporting wafers (approx. 8.0 – 12 mg · cm^{-2}) of the zeolitic materials were pre-treated in situ in quartz IR cell at 450 °C for 2 h under vacuum conditions. A Nicolet 6700 FTIR Spectrometer equipped with an AEM module with a resolution of 4 cm^{-1} was used to record the IR spectra.

The concentration of Brønsted and Lewis acid sites was obtained in quantitative IR studies of d_3-acetonitrile adsorption according to the procedure previously reported [59]. The sample was saturated with d_3-acetonitrile (667 Pa in the gas phase) at room temperature. Then, the sample was evacuated at the same temperature for 20 min to remove the gaseous and physisorbed d_3-acetonitrile molecules. Before adsorption, d_3-acetonitrile was degassed by freezing and thawing cycles. Spectra were recalculated at a wafer density of 10 mg · cm^{-2}. The molar absorption coefficients of d_3-acetonitrile

adsorbed on Brønsted (ε (BAS) $= 2.05 \pm 0.1$ cm $\cdot$ μmol^{-1}) and Lewis (ε (LAS) $= 3.6 \pm 0.2$ cm $\cdot$ μmol^{-1}) acid sites [59] were used to determine the type and concentration of acid sites.

3.4.5   Scanning electron microscopy

Scanning electron microscopy imaging was performed using FEI Quanta 200F. Microscope was equipped with secondary electrons and backscattered electrons detectors. Images were taken at accelerating voltage of 8 kV, using beam spot size 4. Crystals of samples were deposited on the carbon tape mounted on to the SEM holder.

3.4.6   Scanning transmission electron microscopy with energy dispersive X-ray spectroscopy

Scanning transmission electron microscopy imaging was performed using JEOL NEOARM 200F at accelerating voltage of 200 kV. Microscope was equipped with a Schottky-type field emission gun (FEG) and TVIPS XF416 CMOS camera, and annular dark field detector (ADF). The alignment was performed by a standard method using carbon film covered with gold nanoparticles. Samples were deposited at EMR holey carbon support film on copper 300 square mesh. The electron dose was kept at low current density (below 10 pA $\cdot$ cm^{-2}) due to low beam-stability of the samples. Energy dispersive X-ray spectroscopy elemental mapping measurements were acquired using a JEOL JED 2300 EDS analyser.

3.4.7   Inductively coupled plasma mass spectrometry

Silicon, germanium and aluminium contents in zeolite samples were determined by inductively coupled plasma mass spectrometry analysis (Agilent 7900 ICP-MS; Agilent Technologies, Inc., USA). Approximately 50 mg of the sample was mixed with 1.8 ml of nitric acid (ANALPURE®), 5.4 ml of hydrochloric acid (ANALPURE®) and 1.8 ml of hydrofluoric acid (ANALPURE®). The mixture was then transferred into a closed teflon vessel, and heated in the microwave (Speedwave® XPERT, Berghof) at 210 °C (a temperature ramp of 5 °C $\cdot$ min^{-1}) for 25 min. When the sample was cooled down, the complexation of the surplus hydrofluoric acid was done by adding 12 ml of boric acid and further treated in the microwave at 190 °C (a temperature ramp

of 5 °C · min^{-1}) for 10 min. Finally, the obtained cooled down solutions were diluted with Millipore water for analysis.

3.5   Isomerisation of m-xylene

The m-xylene isomerisation reaction experiments were carried out in a Micromeritics microflow Microactivity Effi experimental unit equipped with a stainless-steel fixed-bed reactor (internal diameter 11 mm) in gas phase under atmospheric pressure at 350 °C. Nitrogen was used as a carrier gas (molar fraction of m-xylene in feed was 0.2). Prior to the catalytic experiment, zeolite sample in powder form was pressed into a pellet using pressure of 25 kN. Obtained pellet was grained and then sieved keeping a fraction of particle size of 200 – 500 μm. The zeolite sample (0.5 – 2 g) with particle size 200 – 500 μm was diluted with carborundum (particle size 500 μm, w/w ratio 1/2) and the reactor was filled with this mixture. The apparatus with the reactor was assembled and a leak test at 20 bars for 20 min was performed. Subsequently the pressure was released and the catalyst was activated in a flow of air (100 ml · min^{-1}) at 450 °C for 90 min. After activation, the reaction was flushed with nitrogen and cooled to the temperature of 350 °C. Then, liquid m-xylene (0.26 – 0.7 ml · min^{-1} depending on WHSV) from the reservoir was delivered by an HPLC pump to an evaporator, where the liquid became a vapour and was blended together with nitrogen. This mixture was brought to the catalyst bed. Concentration of m-xylene in the reaction mixture was 20 % vol., flow of nitrogen and m-xylene were calculated according to the mass of the catalyst and selected WHSV (7.7 – 51 h^{-1}). To prevent any condensation of the reactants or products, the temperature in the lines and in the hotbox (a heated box where the reactors, valves and all connecting lines are placed) was maintained at a constant 145 °C. After the reaction, the catalyst was regenerated in a flow of air (200 ml · min^{-1}) at 500 °C for 6 h.

Samples of the reaction mixture were taken and analysed by an online connected Agilent 8890 Gas Chromatography System. The system was equipped with a heated 6-port sampling valve, VF-WAXms column (30m x 0.25mm x 1.00μm) and a TCD-FID serial detectors. The sampling valve temperature was set to 200°C. The analysis was isothermal at 100 °C using a column flow of 0.5 ml · min^{-1} with nitrogen as carrier gas. Temperature of the detectors was 250 °C. The data were evaluated based on FID

detection. In each run, six samples were taken in 20 min intervals, the first analysis started at 15 min time-on-stream.

The parameters that were determined for the catalysts comparison are: conversion of m-xylene [%], yield of a product [%], selectivity [%].

Conversion of m-xylene was determined with assumption of closed mass balance based on equation 3.1, where X is conversion [%], $A_{m\text{-}xylene}$ is an integrated area of the gas chromatography signal for m-xylene and $\Sigma A_{i,\,norm}$ is sum of areas of GC signals for all compounds normalised to the molar response of m-xylene. Normalisation coefficients were determined as ratio of carbon numbers.

$$X = 1 - \frac{A_{m-xylene}}{\Sigma A_{i,norm}} \cdot 100 \ \% \tag{3.1}$$

Yield was determined from the equation 3.2, where Y is the yield [%], $A_{p,norm}$ is an area of GC signal for a product and $\Sigma A_{i,\,norm}$ is sum of areas of GC signals for all compounds normalised to the same molar response of m-xylene (3.2).

$$Y = \frac{A_{p,norm}}{\Sigma A_{i,norm}} \cdot 100 \ \% \tag{3.2}$$

Selectivity was calculated from equation 3.3, where S is selectivity [%], Y_p is yield of a product [%] and X is conversion [%].

$$S = \frac{Y_p}{X} \cdot 100 \ \% \tag{3.3}$$

4 Results and discussion

4.1 Synthesis – ADOR approach

The four-step ADOR method was used for synthesis of the isoreticural IPC family of zeolites. Parent germanosilicate Al-**UTL** zeolite possessing intersecting 14- and 12-ring channel system with germanium atoms preferably in between layers creating double-four-ring units connecting layers was prepared *via* traditional hydrothermal synthesis (Table 2.1) [2]. Germanium rich D4R units connecting layers, were hydrolysed in acidic conditions to obtain a layered precursor – IPC-1P.

Al-IPC-7 material combining two different types of connecting units was synthesised by two-step hydrolysis of parent Al-**UTL**. During the synthetic process, germanium atoms in D4Rs were exchanged for aluminium atoms. Presence of D4R units provides the same size 14- and 12-ring pores as it was in the parent Al-**UTL** zeolite. Single-four-ring units are also a part of Al-IPC-7 sample, and therefore interconnected 12- and 10-ring channels are in the crystals (Table 2.1). Furthermore, additional acid sites were most probably introduced into the framework during the synthetic process.

The formation of S4Rs in between the layers after silylation of IPC-1P produced Al-IPC-2 zeolite. This material contains interconnected 12- and 10-ring channel system (Table 2.1). During the stabilisation step of the synthesis, nitric acid is used. This might lead to the dealumination of the material because the acid treatment is often used to extract aluminium from aluminosilicate framework [65]. Al-IPC-2 zeolite was also prepared by treatment of Al-**UTL** in aluminium nitrate nonahydrate solution. This results in a higher amount of aluminium incorporated in this sample, indicated as 'Al-IPC-2 one-pot'. This sample was prepared to compare the impact of different aluminium content in the same structure, and therefore also the concentration of acid sites on m-xylene isomerisation.

Al-IPC-6 is the second material combining two different types of connecting units. The hydrolysis of parent Al-**UTL** and subsequent treatment leads to the formation of S4Rs and oxygen bridges resulting in interconnected 12- and 10-ring pores, along with 10- and 8-ring pores (Table 2.1). The synthesis of Al-IPC-6 was performed in the aluminium nitrate solution, thus it is possible that more aluminium was incorporated into the framework during this treatment.

The intercalation of octylamine amine was used for the organisation of IPC-1P. Subsequent connection of the layers by calcination led to Al-IPC-4 zeolite. This material with oxygen bridges has interconnected 10- and 8-ring channel system (Table 2.1).

Prepared materials gave the complete spectrum of pore systems for shape selectivity studies of these isoreticular materials in gas phase m-xylene isomerisation reaction. For better understanding they were compared with commercial ZSM-5 catalysts.

4.2 Structural characterisation of materials

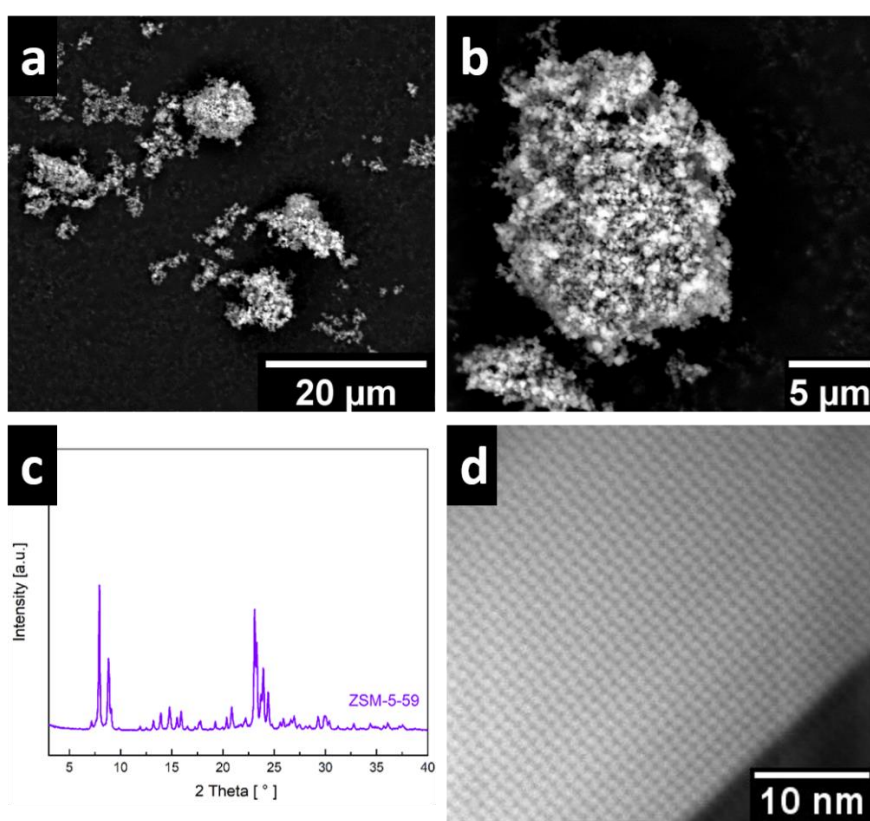### 4.2.1 Commercial ZSM-5 catalyst – structure

Figure 4.1 Characterisation of the commercial ZSM-5 catalyst: (a, b) SEM images, (c) PXRD pattern, (d) STEM image showing characteristic zig-zag pore structure of **MFI**.

Commercial ZSM-5 zeolites were provided by Johnson Matthey Technology Centre. They were Zeolyst CBV5524G and Zeolyst CBV8014 (both in NH_4^+ form). These materials were calcined at 450 °C for 16h to obtain H-form, and denoted as ZSM-5-59 and ZSM-5-93, respectively. The commercial catalysts used as a benchmark for the catalytic test of ADOR zeolites were characterised by PXRD and electron microscopy methods. The morphology and the structure of the commercial ZSM-5-59

crystals are shown in the Figure 4.1. The ZSM-5-59 crystals 0.3 – 1.0 µm in size are agglomerated in bigger domains (Figure 4.1 a, b). The structure of the material was confirmed by the comparison of collected PXRD (Figure 4.1 c) with a good match to the model [1]. Detailed STEM image of the ZSM-5-59 (Figure 4.1 d) also confirmed the structure, showing characteristic zig-zag pore structure of **MFI** type zeolite. STEM image of ZSM-5-59 shows 3D crystals (Figure 4.2 a). Corresponding STEM-EDS mapping analysis of aluminium (blue) and silicon (red) confirms the uniform distribution of these atoms in the ZSM-5-59 structure (Figure 4.2). Aluminium and silicon content were determined by IPC-MS (Table 4.2).
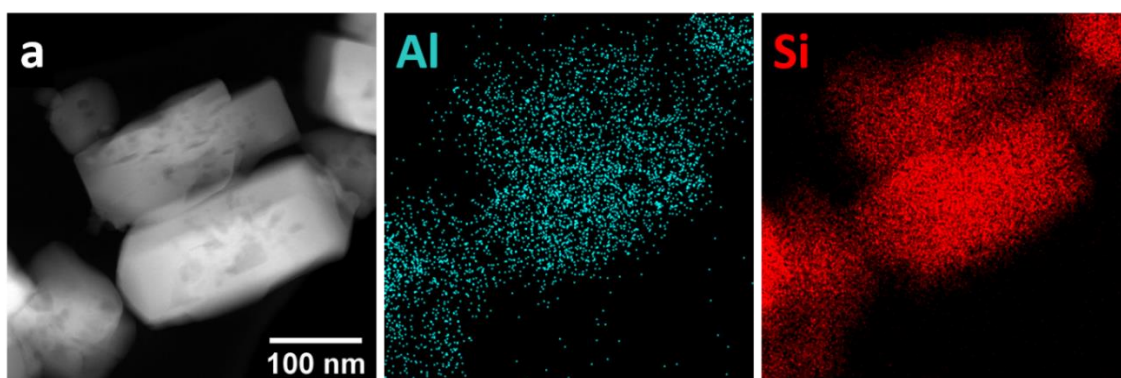

Figure 4.2 STEM image and corresponding EDS elemental distribution maps of aluminium (blue) and silicon (red) in the ZSM-5-59 zeolite crystals.

4.2.2 Structure of ADOR catalysts

The powder X-ray diffraction patterns of parent Al-**UTL** and daughter Al-IPC-n zeolites are shown in the Figure 4.3. PXRDs correspond to the simulated patterns of the model structures [2]. The PXRD patterns confirmed the crystallinity and phase purity for all prepared samples. Interlayer *d*-spacing is decreasing in order: Al-**UTL** (6.15 *2θ*, d-spacing = 1.44 nm) > Al-IPC-7 (7.26 *2θ*, d-spacing = 1.22 nm) > Al-IPC-2 (7.75 *2θ*, d-spacing = 1.14 nm) > Al-IPC-6 (9.12 *2θ*, d-spacing = 0.97 nm) > Al-IPC-4 (9.74 *2θ*, d-spacing = 0.91 nm), it agrees with the shift of the interlayer peak (200) position to higher *2θ* values.
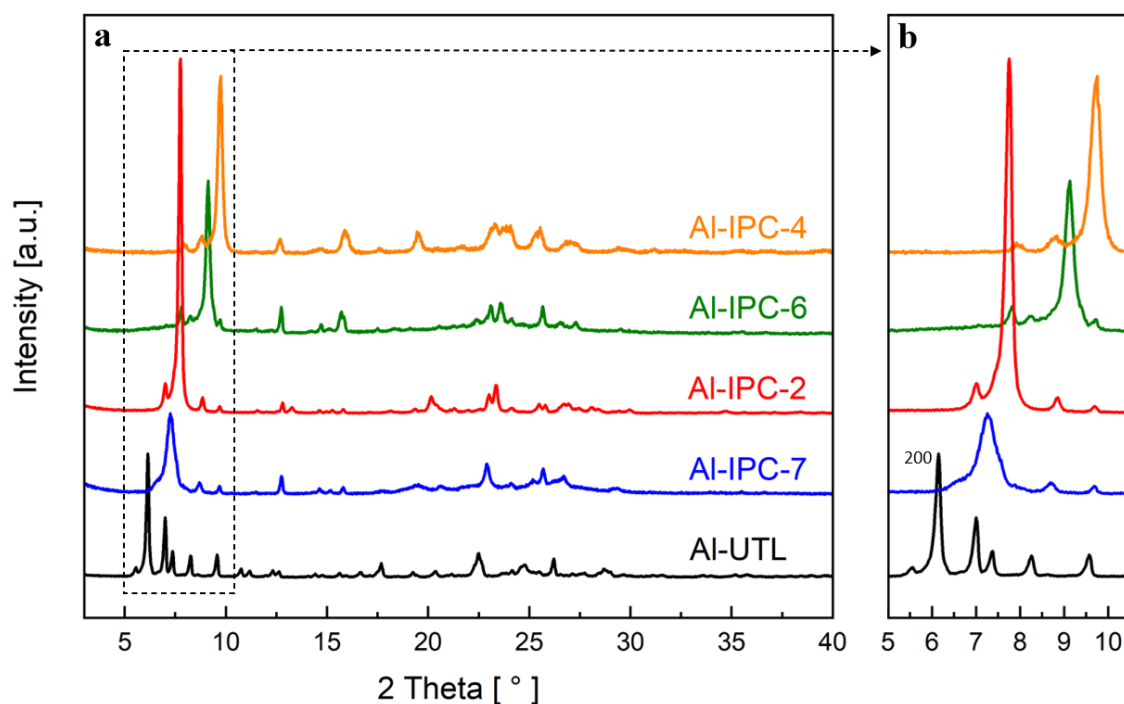
Figure 4.3 (a) PXRD patterns of the parent Al-**UTL** and daughter Al-IPC-7, Al-IPC-2, Al-IPC-6 and Al-IPC-4 zeolites, and (b) low-angle region showing the most intensive interlayer (200) peaks.

Scanning electron microscopy images are shown in the Figure 4.4. Crystal morphology and size were determined for each synthesised material. Al-IPC-2 zeolite possesses approx. 10 µm plate-like rectangular crystals (Figure 4.4 e, f) resembling the parent Al-**UTL** crystals (Figure 4.4 a, b). Al-IPC-2 (Figure 4.4 e) tends to agglomerate more than Al-**UTL** (Figure 4.4 a). In the case of Al-IPC-7, it is evident that the crystals differ in size and they agglomerate (Figure 4.4 c). However, in the magnified image (Figure 4.4 d) plate-like morphology similar to the parent Al-**UTL** is shown. Morphologies and sizes of Al-IPC-7 (Figure 4.4 c, d) and Al-IPC-6 (Figure 4.4 g, h) crystals look alike due to almost identical synthetic processes. Big agglomerates (approx. 40 µm) of Al-IPC-4 (Figure 4.4 i, j) having plate-like rectangular morphology correspond to the nature of the parent Al-**UTL** material.
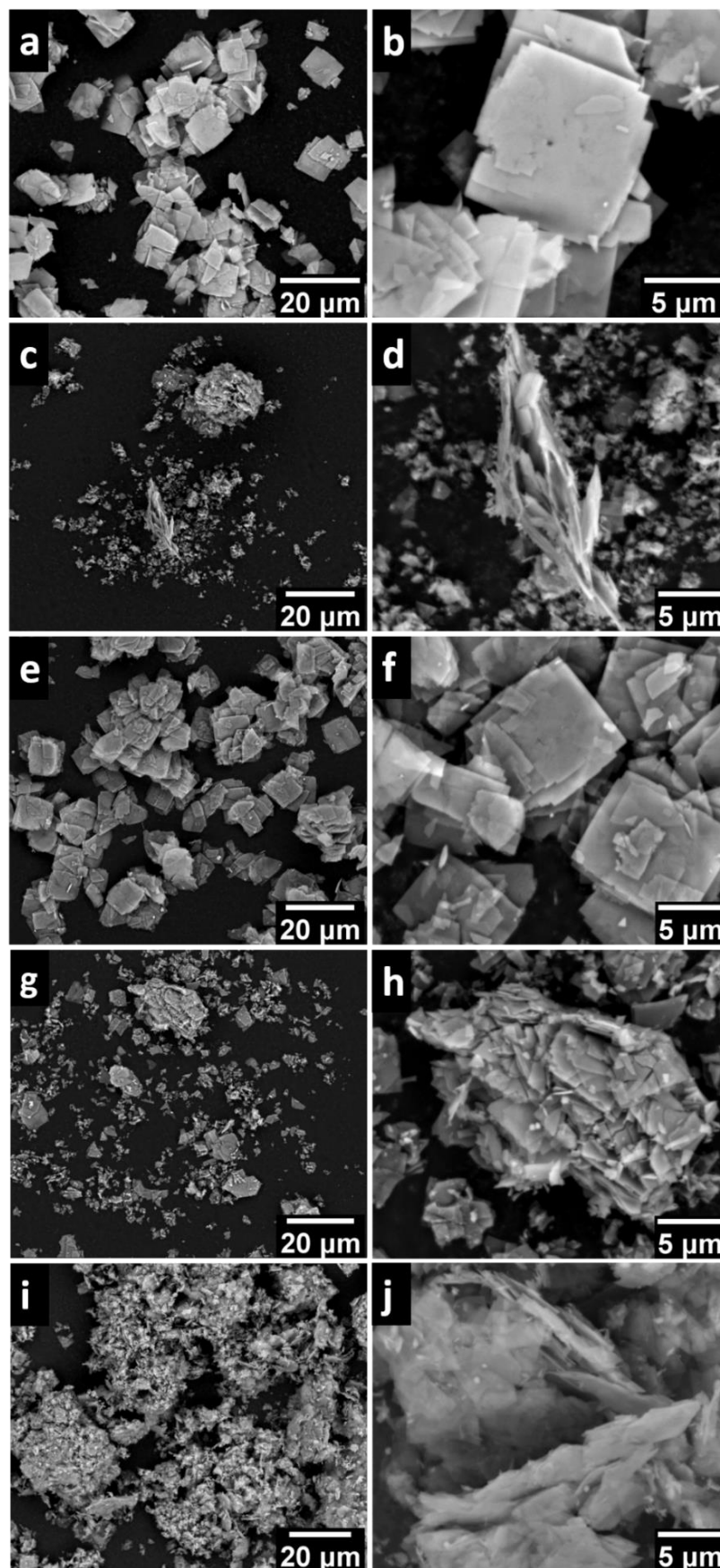
Figure 4.4 SEM images of synthesised ADOR zeolites: (a, b) Al-**UTL**, (c, d) Al-IPC-7, (e, f) Al-IPC-2, (g, h) Al-IPC-6 and (i, j) Al-IPC-4.

Comparison of SEM images of Al-IPC-2 zeolites synthesised using two different methods is shown in the Figure 4.5. The Al-IPC-2 crystals prepared by ADOR route (Figure 4.5 a, b) are rectangular with plate-like morphology (approx. 3 – 10 μm crystals) resembling the morphology of a parent Al-**UTL** zeolite, whereas Al-IPC-2 one-pot crystals (Figure 4.5 c, d) agglomerate having also significant amount of smaller (≤ 2.5 μm), non-uniform shape domains. Nevertheless, there are still some similarities between these samples, *e.g.* sample prepared by one-pot synthesis contains larger rectangular crystals (Figure 4.5 d) comparable with those present in the Al-IPC-2 ADOR.
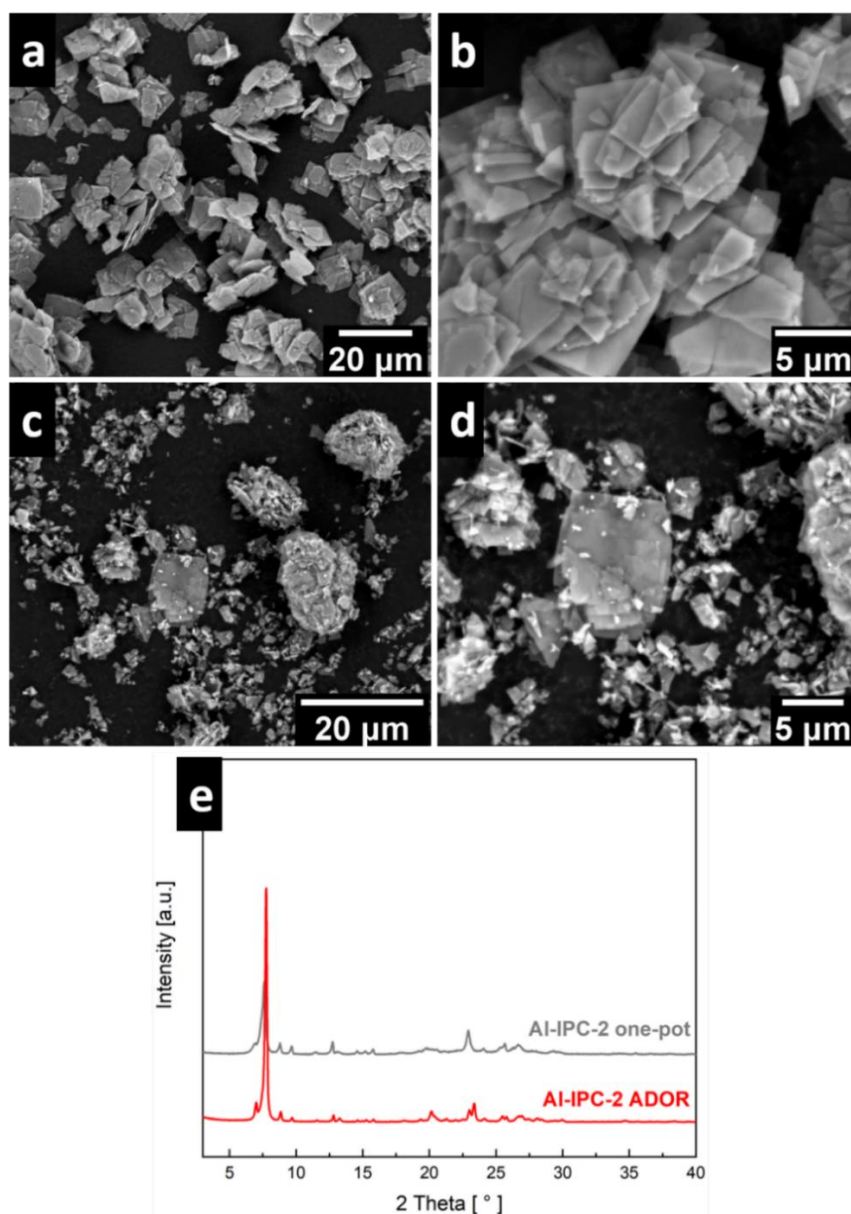
Figure 4.5 Comparison of the structure and morphology of AL-IPC-2 type material prepared by standard ADOR and one-pot method. SEM images of Al-IPC-2 zeolite prepared using (a, b) ADOR method and (c, d) one-pot synthesis, (e) PXRD patterns.
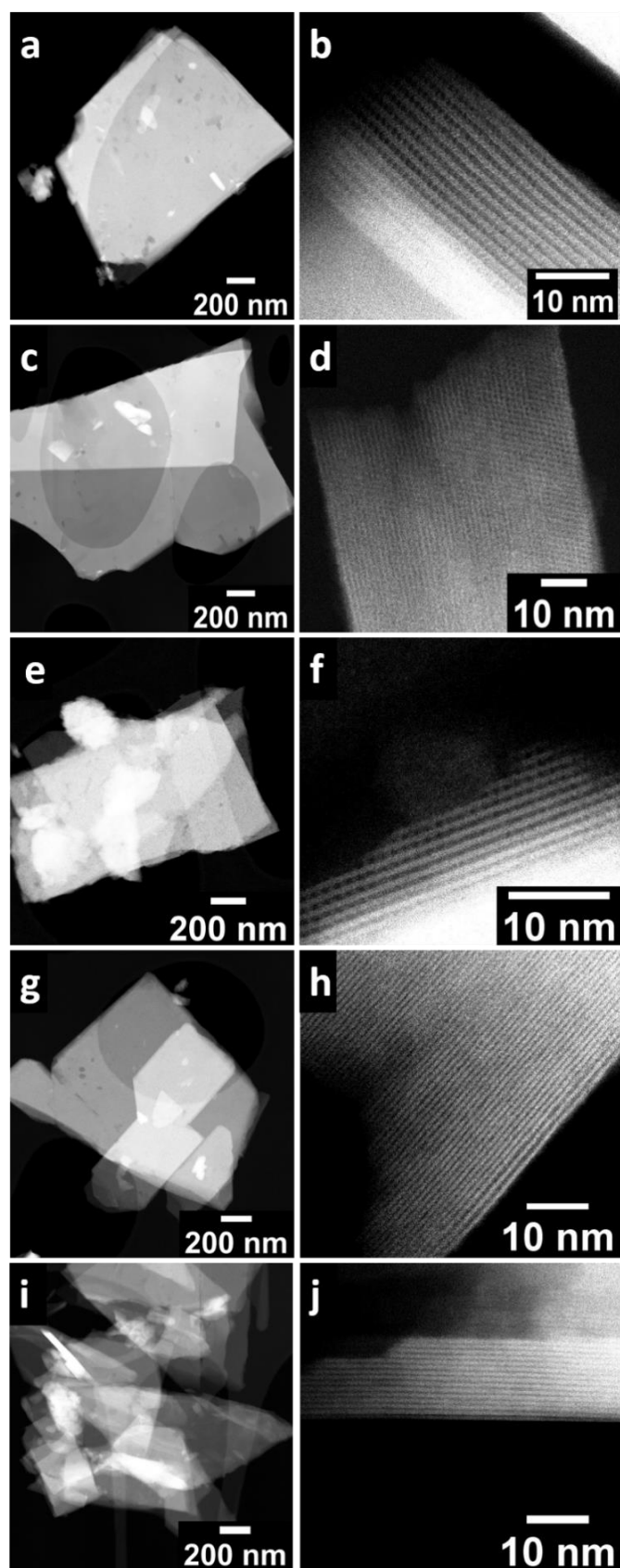
Figure 4.6 STEM images of crystal from the top (left) and side-view showing the interlayer spacings (right) of ADOR zeolites: (a, b) Al-**UTL**, (c, d) Al-IPC-7, (e, f) Al-IPC-2, (g, h) Al-IPC-6 and (i, j) Al-IPC-4.

Based on the scanning transmission electron microscopy (STEM) images (Figure 4.6), thin plate-like crystal morphology is observed in all prepared ADOR zeolite samples. This corresponds to SEM imaging (Figure 4.4). Figure 4.6 e, i shows smaller agglomerated crystal fragments in Al-IPC-2 and Al-IPC-4 samples, this can be explained by the similar first step of their synthesis, hydrolysis of parent Al-**UTL** in acetic acid. Figure 4.6 (right) shows high-resolution side view images of representatives of IPC zeolite family crystals. In these images, it is possible to observe the crystalline layers, as well as interlayer spacings, and the pore systems of each representative of ADOR zeolites. The interlayer *d*-spacings calculated based on these images are corresponding to those calculated from the position of dominant peak in the PXRDs (Figure 4.3) which confirmed the formation of presumed structures prepared by ADOR synthesis.
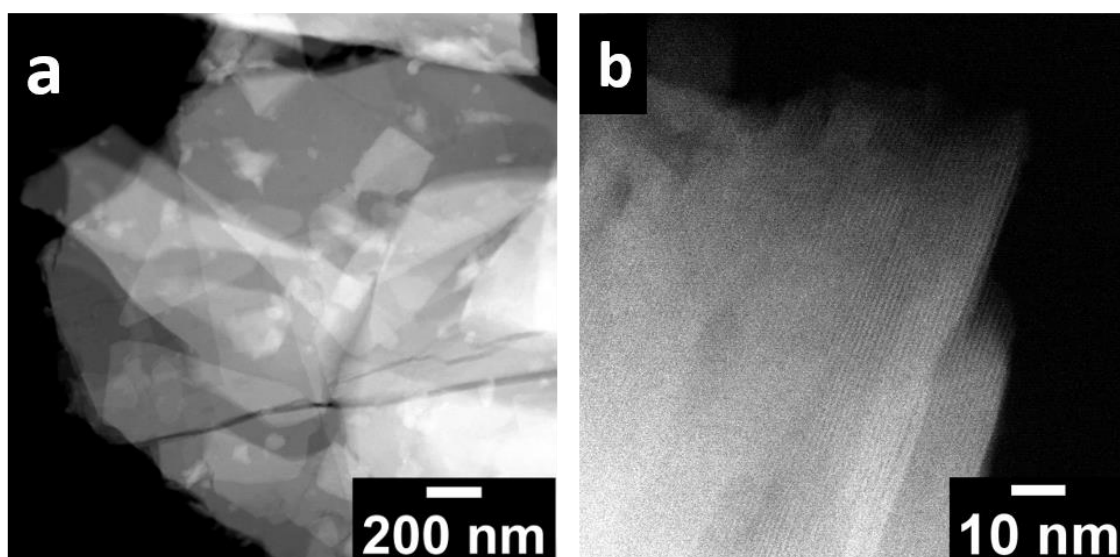
Figure 4.7 STEM images of (a) crystal morphology and (b) interlayer spacing of Al-IPC-2 prepared by one-pot method.

Crystals of Al-IPC-2 one-pot sample possess plate-like morphology, they are fragmented and agglomerated at the same time (Figure 4.7). The resemblance between crystals of Al-IPC-2 one-pot (Figure 4.7 a) and Al-IPC-2 ADOR (Figure 4.6 e) can be explained by the same type of their IPC-2 structure. Crystal from side-view (Figure 4.7 b) shows interlayer spacing of Al-IPC-2 sample corresponding with the model.

STEM images with corresponding EDS maps of ADOR zeolites show uniform distribution of germanium, aluminium, and silicon in the analysed crystals (Figure 4.8).

Figure 4.8 STEM images and EDS elemental distribution maps of: germanium (green), aluminium (blue), and silicon (red) for isoreticular zeolites prepared using ADOR approach: (a) Al-**UTL**, (b) Al-IPC-7, (c) Al-IPC-2, (d) Al-IPC-6 and (e) Al-IPC-4.

As expected, the highest amount of germanium is incorporated in the parent Al-**UTL** structure (Figure 4.8 a, green, Table 4.2). The content of germanium in daughter zeolites is reduced due to the selective removal of germanium in their synthetic processes (Figure 4.8 b – e, green), however the presence of germanium is still visible with uniform

distribution. This can point to the fact, that nevertheless, germanium preferentially occupies D4R units, some of germanium is also integrated in the layers. We expected that the aluminium content in Al-**UTL** is the lowest (Figure 4.8 a, blue) in contrast to Al-IPC-n materials (Figure 4.8 b – e, blue) which is confirmed. The silicon content in the framework does not change, the slight changes in density of silicon in the maps are the result of the overlap of crystals (Figure 4.8 a – e, red).

Analysis of Al-IPC-2 one-pot crystals by STEM-EDS elemental mapping confirms the uniform distribution of germanium, aluminium, and silicon in the sample (Figure 4.9). Nevertheless, in case of aluminium, some parts of the crystals show the slight local agglomeration of this element. Based on the aluminium distribution maps, we assume, that most probably it is a sign of the presence of the extra-framework aluminium or agglomeration of aluminium on the surface of crystals of Al-IPC-2 one-pot zeolite (Figure 4.9, blue).
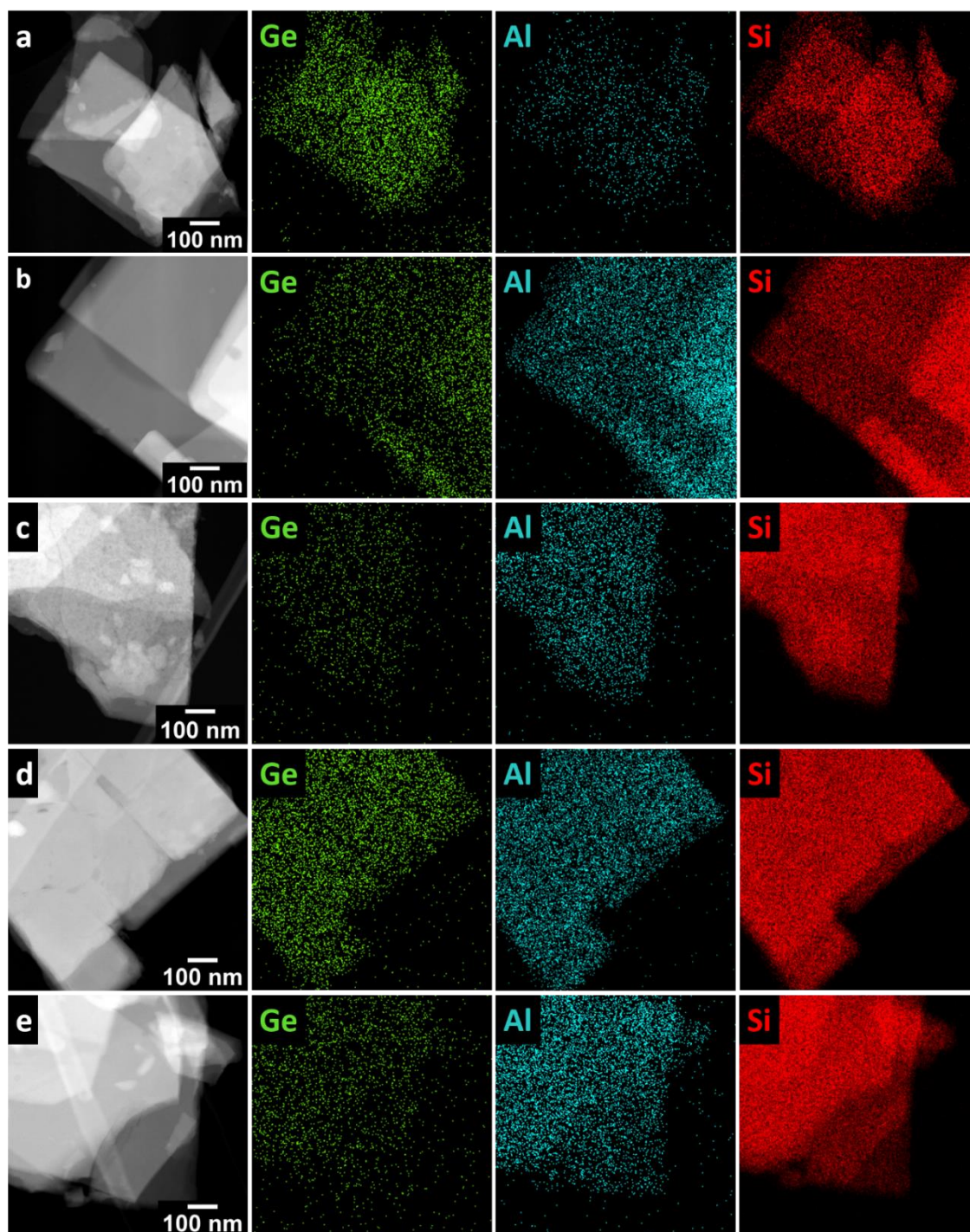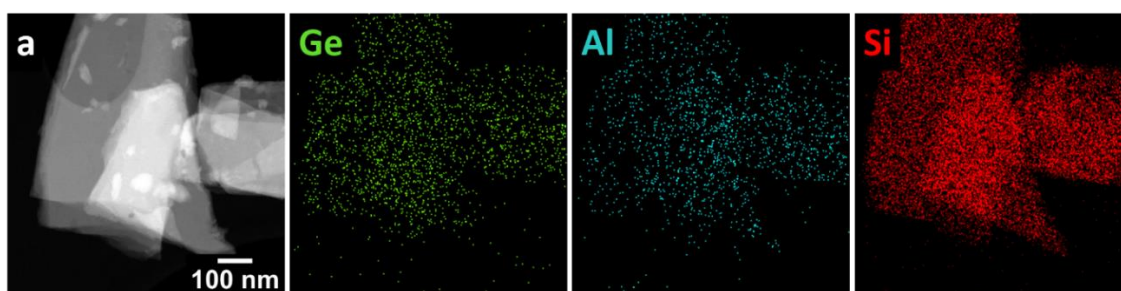

Figure 4.9 STEM image and EDS elemental distribution maps of: germanium (green), aluminium (blue), and silicon (red) for Al-IPC-2 one-pot sample.

4.3   Texture of used catalysts

Textural properties of prepared catalysts were determined by the argon sorption at -186.15 °C. Argon was chosen as the sorbent due to size of its molecules (with smaller diameter than nitrogen). This made possible a more precise investigation of smaller pores in Al-IPC-6 and Al-IPC-4 zeolites (10-ring and 8-ring interconnected channels). The increase in the argon amount adsorbed at lower than 0.1 relative pressures is caused by fast filling of micropores (Figure 4.10). Average pore size of prepared zeolites is decreasing in order: Al-**UTL** > Al-IPC-7 > Al-IPC-2 = Al-IPC-2 one-pot > Al-IPC-6 > Al-IPC-4, which corresponds to the structure and channel sizes (Table 4.1).

Figure 4.10 Argon adsorption and desorption isotherms for (black) Al-**UTL**, (dark blue) Al-IPC-7, (red) Al-IPC-2 ADOR, (green) Al-IPC-6, (orange) Al-IPC-4, (grey) Al-IPC-2 one-pot, (violet) ZSM-5-93 and (sky blue) ZSM-5-59 at –186.15 °C.
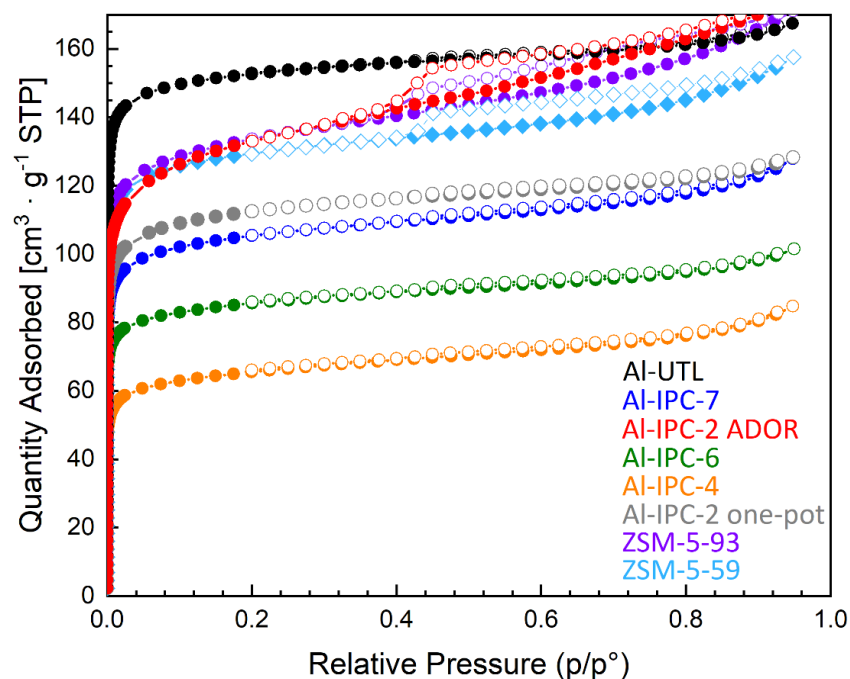
Experimentally determined micropore volumes generally agree with the theoretical pore sizes of prepared materials (Table 4.1). However, calculated BET area for Al-IPC-2 ADOR has higher values than for Al-IPC-7 (Figure 4.10, Table 4.1) which was not expected. Also, hysteresis loop is present in the Al-IPC-2 ADOR isotherm, which indicates the presence of mesopores or defects due to non-perfect reassembly of the layers in this sample. It might be caused by the treatment of the sample with 1M nitric acid, which was used in one of the synthesis steps. Moreover, crystals of Al-IPC-2 ADOR sample create lumps (Figure 4.4 e). Thus, it is possible that the formation of hysteresis loop in the isotherm is caused by the intercrystalline adsorption in such agglomerates. It means that adsorbed argon fills the voids created in between lumps of crystals.

Textural properties of the commercial ZSM-5-93 catalyst are comparable to values obtained for synthesised catalysts (Al-**UTL**, Al-IPC-n). However, the commercial ZSM-5-59 possesses higher total pore volume and micropore volume (Table 4.1) than the other catalysts.

Table 4.1 Textural properties of ADOR zeolites (parent Al-**UTL**, Al-IPC-n), Al-IPC-2 one-pot and ZSM-5 samples determined by argon sorption measurement at –186.15 °C.

Zeolite	BET Surface Area [$m^2 \cdot g^{-1}$]	Total Pore Volume [$cm^3 \cdot g^{-1}$]	Micropore Volume [^{a}] [$cm^3 \cdot g^{-1}$]	Average Pore Size [^{a}] [nm]
Al-**UTL**	455	0.18	0.18	0.86
Al-IPC-7	317	0.14	0.11	0.65
Al-IPC-2	402	0.18	0.12	0.63
Al-IPC-6	257	0.10	0.09	0.50
Al-IPC-4	198	0.09	0.07	0.47
Al-IPC-2 one-pot	337	0.14	0.11	0.63
ZSM-5-93	402	0.16	0.14	0.65
ZSM-5-59	386	0.26	0.21	0.54

^{a} NLDFT method

Inductively coupled plasma mass spectrometry was utilised for the elemental analysis of prepared zeolites to determine the molar ratios of silicon to aluminium (Si/Al) and silicon to germanium (Si/Ge) (Table 4.2). The germanium content is the highest in the Al-**UTL** sample (Si/Ge = 2.8). The higher Si/Ge measured for the daughter materials confirms the selective removal of germanium from the Al-**UTL** framework during the synthesis of IPC-n zeolites. The lowest germanium content was measured for samples prepared *via* layered precursor: Al-IPC-2 (ADOR) and Al-IPC-4 which corresponds to the assumption that the most effective removal of germanium is realised in acid solution (disassembly to IPC-1P in 1M acetic acid).

On the other hand, aluminium content in Al-**UTL** zeolite is the lowest, which corresponds to the obtained value for the concentration of acid sites in this sample (Table 4.3). The highest concentrations of aluminium are observed for the Al-IPC-7, Al-IPC-6 and Al-IPC-2 one-pot (decreasing order) (Table 4.2). The aluminium content of Al-IPC-7 is unexpectedly high, and it may be due to several reasons. Most probably, it is caused by treatment of parent Al-**UTL** with aluminium nitrate nonahydrate solution during the synthetic processes of these zeolites. During this treatment, some germanium from parent Al-**UTL** might be exchanged to aluminium, that was incorporated into the framework. Another cause might be the formation of extra-framework aluminium. The obtained value of aluminium content for Al-IPC-2 ADOR is the lowest among all prepared catalysts, this corresponds to measured concentration of acid sites in Al-IPC-2

ADOR using acetonitrile adsorption followed by FTIR measurement (Table 4.2, Table 4.3), this is the outcome of the synthesis process involving the treatment with acid solution. In the case of Al-IPC-2 ADOR synthesis, there was no additional source of aluminium used in any of the steps. Thus, all aluminium present in this sample originate from the parent Al-**UTL**.

Table 4.2 Aluminium content [mmol · g^{-1}], molar ratio of silicon to aluminium and silicon to germanium of ADOR zeolites, Al-IPC-2 one-pot and ZSM-5 zeolites determined by ICP-MS.

Zeolite	Al [mmol · g^{-1}]	Si/Al	Si/Ge
Al-**UTL**	0.11	53.7	2.8
Al-IPC-7	3.02	3.1	23.3
Al-IPC-2 ADOR	0.15	78.6	117.9
Al-IPC-6	0.48	23.1	24.0
Al-IPC-4	0.17	66.6	108.2
Al-IPC-2 one-pot	0.36	27.6	8.2
ZSM-5-93	0.29	36.1	n.a.[a]
ZSM-5-59	0.33	25.8	n.a.[a]

[a] ZSM-5 samples did not contain germanium

4.4   Characterisation of acid sites

The investigation of acid sites in the prepared series of catalysts: Al-**UTL**, Al-IPC-n, commercial ZSM-5-59 and ZSM-5-93 was done using deuterated acetonitrile adsorption followed by FTIR measurements (Figure 4.11). The type and concentration of acid sites were determined using d_3-acetonitrile due to its suitable kinetic diameter for accessibility to 10- ring and 8-ring interconnected pores in Al-IPC-6 and Al-IPC-4 zeolites. The significantly highest concentration of acid sites is in the Al-IPC-7 sample. This corresponds with the ICP-MS analysis results. Most probably, this is caused by the treatment with the most concentrated aluminium nitrate solutions (Figure 4.11, Table 4.3). The excess of aluminium nitrate might not be washed after the treatment. Also, the concentration of LAS and BAS in Al-IPC-2 one-pot sample is high, most probably due to the use of additional aluminium source during the synthesis (Table 4.3). We assume that during these treatments germanium atoms of parent Al-**UTL** were

substituted by aluminium, that possibly was incorporated into the zeolite framework. The acidity of those samples is substantially higher that of remaining samples, thus it is presumed that some aluminium was integrated into the sample as extra-framework species. This hypothesis is also supported by the elemental analysis (especially high content of aluminium is in the Al-IPC-7). No extra phases that would suggest the impurities are observed in the PXRD, however, SEM and STEM images of Al-IPC-7 and Al-IPC-2 one-pot show small debris located on the zeolite crystals. However, the precise description of the possible extra framework aluminium would require additional experiments, *e.g.* ^{27}Al solid state NMR.

On the other hand, IPC-2 prepared by conventional ADOR method contains the lowest total number of acid sites (Table 4.3). This interesting result is most likely caused by the presence of 1M nitric acid in the stabilisation step of the synthesis that is performed in the hydrothermal conditions (in autoclave at 175 °C for 16 h), causing dealumination of the material. The acid treatment of aluminosilicates is frequently used for the extraction of aluminium from framework [65]. Selective removal of germanium atoms from Al-**UTL** is the key step for the preparation of ADOR Al-IPC-n materials. Therefore, Al-**UTL** possesses relatively lower concentration of acid sites compared to its daughter zeolites Al-IPC-7, Al-IPC-6 and Al-IPC-4 (except for Al-IPC-2). Acid centres are crucial for catalytic reactions. Therefore, based on these observations, differences in the acid strength of prepared zeolite catalysts are expected to affect their behaviour in m-xylene isomerisation.

Table 4.3 Concentration of Brønsted and Lewis acid sites from IR studies of d_3-acetonitrile sorption. The concentrations were calculated from the area of band at 2330 cm^{-1}, 2312 cm^{-1} (LAS$_{strong}$ and LAS$_{weak}$) and 2300 cm^{-1} (BAS) using the absorption coefficient from Ref [59].

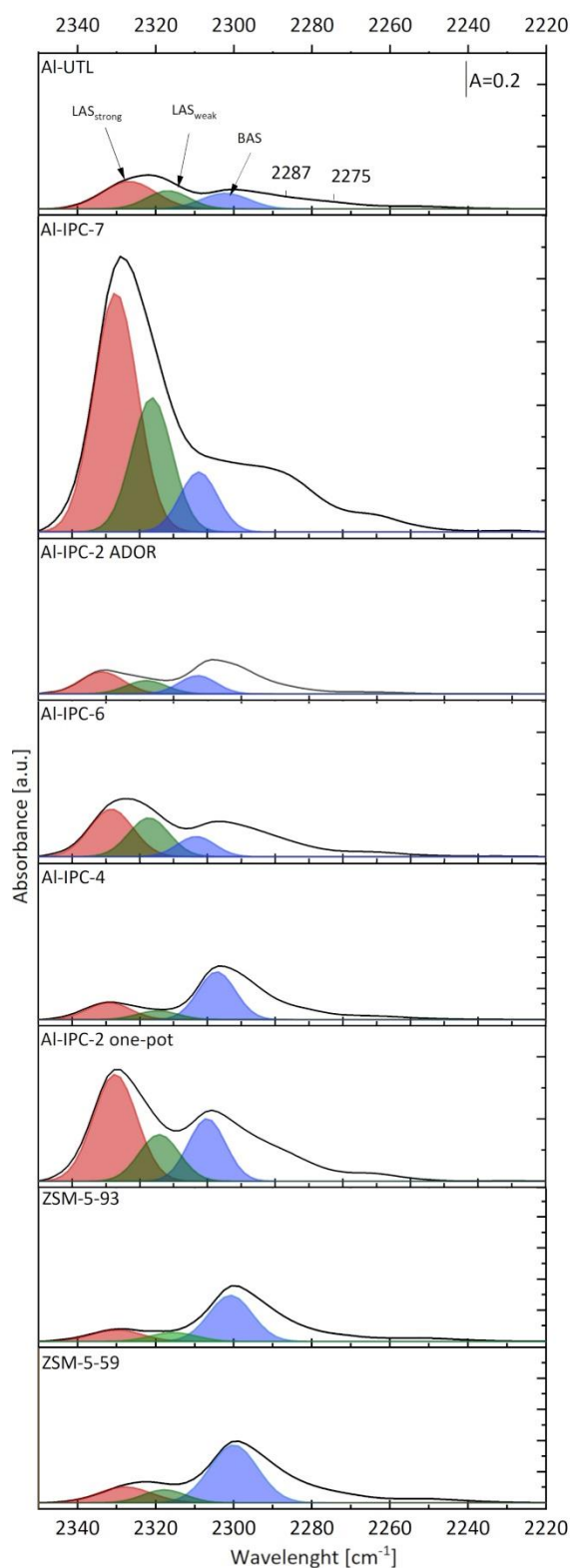| Zeolite	BAS [mmol · g^{-1}]	LAS$_{strong}$ [mmol · g^{-1}]	LAS$_{weak}$ [mmol · g^{-1}]	LAS [mmol · g^{-1}]	BAS + LAS [mmol · g^{-1}]
Al-**UTL**	0.042	0.037	0.025	0.062	0.104
Al-IPC-7	0.128	0.339	0.175	0.514	0.642
Al-IPC-2 ADOR	0.040	0.032	0.018	0.05	0.090
Al-IPC-6	0.044	0.069	0.052	0.121	0.165
Al-IPC-4	0.104	0.025	0.012	0.037	0.141
Al-IPC-2 one-pot	0.136	0.154	0.062	0.216	0.352
ZSM-5-93	0.201	0.033	0.024	0.057	0.258
ZSM-5-59	0.282	0.075	0.031	0.106	0.388

Figure 4.11 FTIR spectra of d_3-acetonitrile adsorbed in Al-**UTL**, Al-IPC-7, Al-IPC-2, Al-IPC-6, Al-IPC-4 prepared by ADOR method, Al-IPC-2 one-pot and commercial ZSM-5-93 and ZSM-5-59 zeolite catalysts; peaks were deconvoluted to show the share of LAS$_{strong}$ (red), LAS$_{weak}$ (green), BAS (blue) in overall acidity [59].

4.5 Influence of the pore structure in m-xylene isomerisation

The aluminium containing ADOR zeolites (parent Al-**UTL**, Al-IPC-7, Al-IPC-2, Al-IPC-6 and Al-IPC-4), Al-IPC-2 sample prepared by one-pot synthesis, and the conventional ZSM-5 catalysts (benchmark material) were tested in gas phase m-xylene isomerisation at 350 °C. The prepared catalysts differ in the pore system. Crystalline layers are connected with various interlayer units, resulting in a different pore system for each catalyst: 14- x 12-ring (Al-**UTL**), 14- x 12-ring with 12- x 10-ring (Al-IPC-7), 12- x 10-ring (Al-IPC-2), 12- x 10- ring with 10- x 8-ring (Al-IPC-6) and 10- x 8-ring (Al-IPC-4) (Table 2.1). These catalysts also differ in the concentrations of acid sites (Table 4.2), which act as the active sites in the m-xylene isomerisation.

The reaction was carried out in a microflow stainless-steel fixed-bed reactor in gas phase under atmospheric pressure with nitrogen as a carrier gas. The conditions were optimised to compare the performance of prepared catalysts with commercial ZSM-5 at similar conversion. For comparison, following parameters were used: m-xylene conversion [%], selectivity to p-xylene [%], ratio between disproportionation and isomerisation reactions, ratio between p-xylene and o-xylene yield, yield of trimethylbenzenes and time-on-stream [min].

4.5.1 Optimisation of the catalytic experiments

First pilot experiments with Al-**UTL** and ZSM-5-59 were at WHSV 41 h^{-1} and 350 °C (Figure 4.12 a). Conversion over Al-**UTL** is significantly lower (below 1 %) during the whole experiment than over ZSM-5 (40.6 % at 25 min T-O-S). It is not possible to compare Al-**UTL** and ZSM-5-59 at these starting conditions (WHSV 41 h^{-1} and 350 °C), therefore prior to the catalysts testing, optimisation of reaction conditions (WHSV and temperature) was performed. Experiments at WHSV 31 h^{-1} and 51 h^{-1} at the same temperature (350 °C) were done (Figure 4.12 a). Conversion of m-xylene over Al-**UTL** at WHSV 51 h^{-1} was below 0.5 % during the whole experiment and at WHSV 31 h^{-1} increased to 2.3 % at 25 min T-O-S (Figure 4.12 a). Conversion increased with decreasing WHSV. In order to increase conversion over Al-**UTL**, WHSV 19 h^{-1} was tested resulting in 20.8 % conversion at 25 min T-O-S (Figure 4.12 a). The WHSV equal to 7.7 h^{-1} was examined to increase conversion over Al-**UTL** even more with aim to observe the most similar values of conversion over Al-**UTL** and commercial ZSM-5-59 (Figure 4.12 a).

Al-**UTL** gives the highest conversions of m-xylene at WHSV of 7.7 h^{-1} (43.8 % at 25 min T-O-S) and 19 h^{-1} (20.8 % at 25 min T-O-S). To decrease m-xylene conversion over ZSM-5-59, a lower reaction temperature of 300 °C was examined (Figure 4.12 b). In spite of lower temperature, significant change in conversion over ZSM-5-59 was not observed. Values chosen as optimum condition for the catalytic experiments study were WHSV 7.7 h^{-1} and 19 h^{-1}, and temperature 350 °C (Figure 4.12 highlighted in red).

For the study of the shape selectivity effect ZSM-5-93 sample was used instead of ZSM-5-59 sample, because aluminium content in ZSM-5-93 is closer to that of prepared isoreticular zeolites (Table 4.2). The optimisation data are valid for ZSM-5-93 as well since the conversion values were almost the same, conversion over ZSM-5-59 (40.6 % at 25 min T-O-S) used in optimisation process (Figure 4.12 a) and over ZSM-5-93 (38.2 % at 25 min T-O-S) used for catalytic testing (Figure 4.13 a).

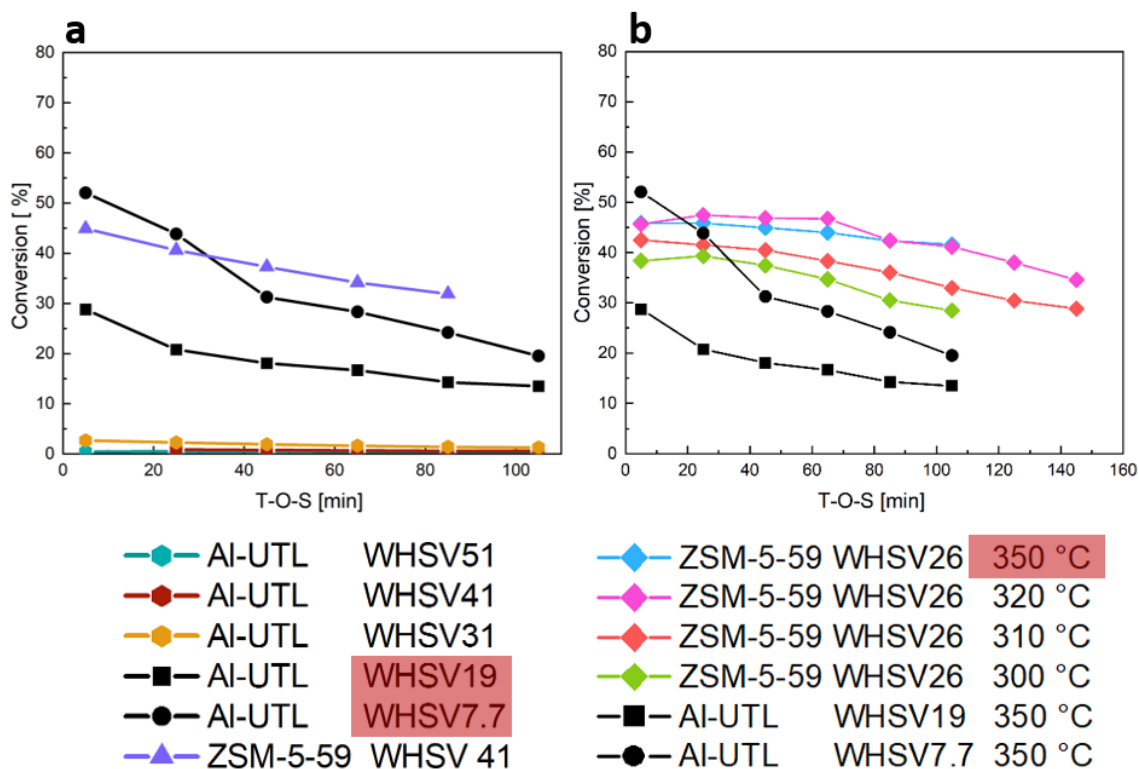**Figure 4.12** Time-on-stream dependence of m-xylene conversion over (a) Al-**UTL** at different WHSVs (7.7 – 51 h^{-1}) at 350 °C; ZSM-5-59 at WHSV 41 h^{-1} serves as benchmark; (b) ZSM-5-59 at WHSV 26 h^{-1} and various temperatures (300 – 350 °C); Al-**UTL** at WHSV 7.7 h^{-1} and 19 h^{-1}, and 350 °C serve as benchmarks.

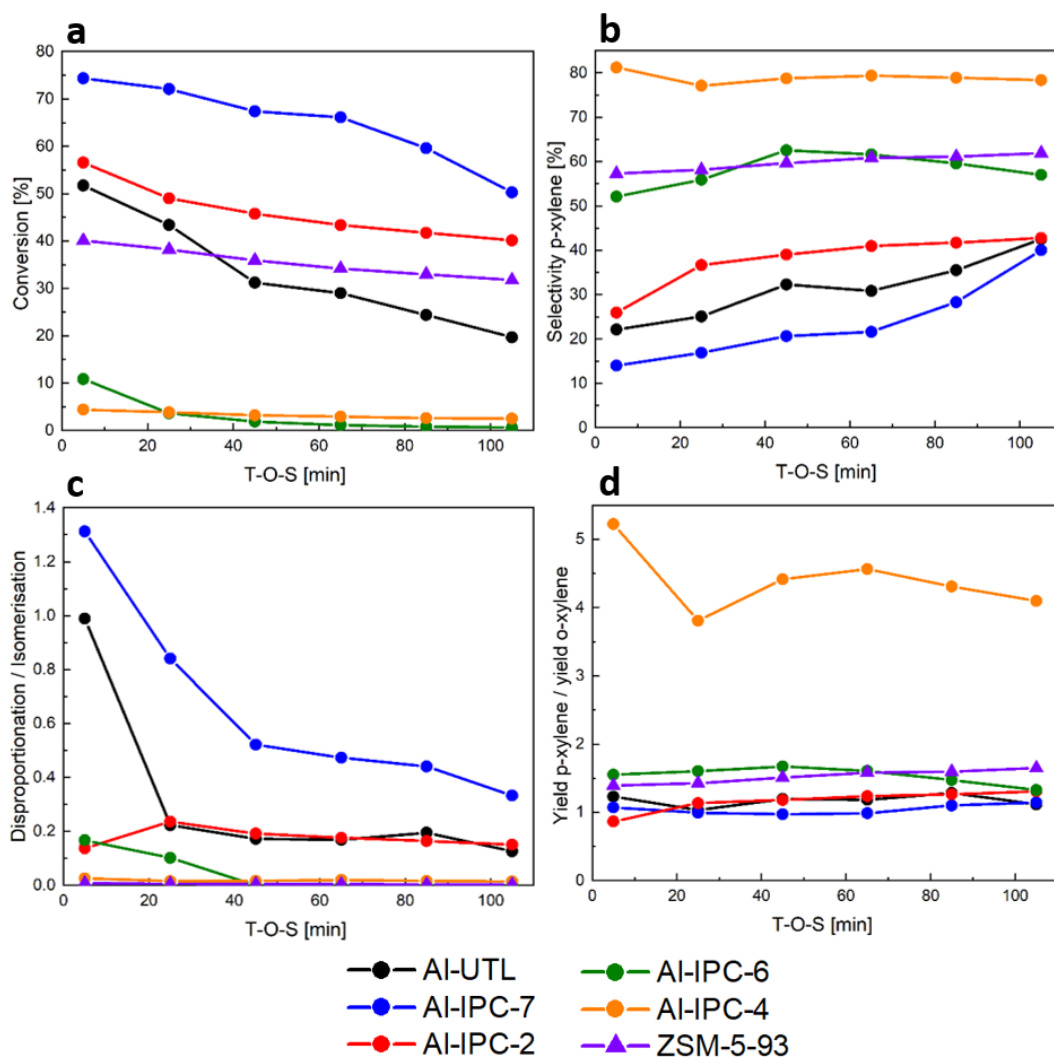## 4.5.2 Catalytic experiments at WHSV 7.7 h^{-1}

Figure 4.13 Time-on-stream dependence of (a) m-xylene conversion, (b) selectivity of p-xylene, (c) ratio between disproportionation (yield of toluene) and isomerisation (yield of p-xylene plus yield of o-xylene) reactions (d) ratio between p-xylene and o-xylene yield in m-xylene isomerisation over Al-**UTL**, Al-IPC-7, Al-IPC-2 (ADOR mechanism preparation), Al-IPC-6 catalysts at WHSV 7.7 h^{-1} and 350 °C; Al-IPC-4 was measured at WHSV 9.6 h^{-1} and 350 °C; ZSM-5-93 at WHSV 41 h^{-1} and 350 °C serves as benchmark.

Isoreticular zeolites showed high conversions at WHSV 7.7 h^{-1}. Figure 4.13 shows results of the catalytic experiments with Al-**UTL** and AL-IPC-n at WHSV 7.7 h^{-1} (except for Al-IPC-4 – WHSV 9.6 h^{-1}) catalysts compared to commercial ZSM-5-93 at WHSV 41 h^{-1} and at 350 °C in m-xylene isomerisation. Conversion of m-xylene

increases in a following order: Al-IPC-4 < Al-IPC-6 < Al-**UTL** < Al-IPC-2 < Al-IPC-7 (Figure 4.13 a). Al-IPC-7 shows the highest conversion of m-xylene (Figure 4.13 a) due to the highest content of acid centres combined with the pore sizes of the zeolites (Table 4.3). Interestingly, the conversion over Al-IPC-2 ADOR (49.0 % at 25 min T-O-S) sample is higher than over Al-**UTL** (43.9 % at 25 min T-O-S), although Al-IPC-2 ADOR does not possess higher concentration of acid sites than Al-**UTL** (Table 4.3**).** This might be caused by some diffusion effects or difference of accessibility of the acid sites. Further analysis would require more experiments not possible to perform due to time limitation. Conversions over Al-IPC-6 (3.6 % at 25 min T-O-S) and Al-IPC-4 (3.8 % at 25 min T-O-S) are the lowest even though their concentration of acid sites and aluminium content are comparable or even higher compared to Al-**UTL** and Al-IPC-2 ADOR (Table 4.2, Table 4.3) which provided higher conversion (Al-**UTL** 43.9 % at 25 min T-O-S) (Al-IPC-2 ADOR 49.0 % at 25 min T-O-S). Aluminium content and also pore system of the catalysts strongly influence m-xylene isomerisation reaction. Pore size effect prevails over the effect of acid sites (aluminium content) in m-xylene isomerisation over Al-IPC-6 and Al-IPC-4 catalysts. As a result, the lowest conversions are observed when using these materials. On top of that, 8-ring pores, which are part of interconnected 10- and 8-ring channel system of Al-IPC-4 zeolite, are too narrow thus inaccessible for xylenes molecules, therefore these channels behave like if they were not present. Furthermore, practical decrease of the channel dimensionality in Al-IPC-4 from 2D system to 1D system creates diffusion obstacles and thus further decreases the conversion (Figure 4.13 a and Figure 4.14 a).

Two reaction pathways are possible for m-xylene isomerisation, monomolecular and bimolecular mechanisms (Figure 2.3). Monomolecular isomerisation is a primary reaction in case of xylenes and gives high yields of p-xylene, although also o-xylene can be formed. For this type of a reaction mechanism, confinement is preferred, which means that the reaction occurs in rather narrow pores (10-ring channels) [8, 10]. On the other hand, bimolecular disproportionation which is confinement suppressed (bimolecular transition state cannot be formed in the narrow pores) and thus favoured in 12-ring and larger channels. Trimethylbenzenes, toluene and benzene are other possible products in this reaction system [8, 10, 46]. Both groups of reactions, isomerisation and disproportionation, are catalysed by BAS and LAS [8]. The order in terms of selectivity to p-xylene is opposite compared to conversion (Figure 4.13 b), but selectivities need to be compared at the same conversion for their valid comparison, see Figure 4.15 b.

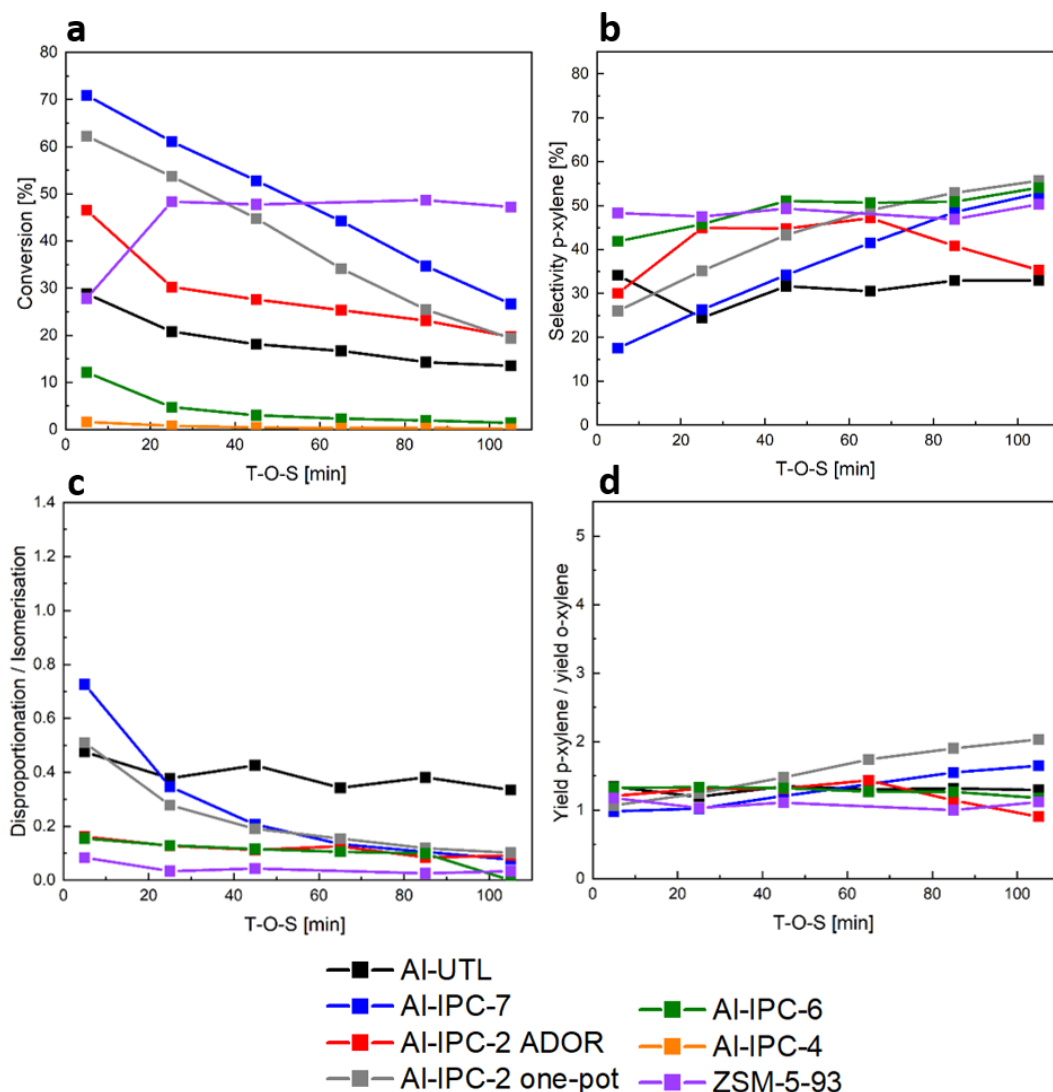## 4.5.3 Catalytic experiments at WHSV 19 h^{-1}

Figure 4.14 Time-on-stream dependence of (a) m-xylene conversion, (b) selectivity to p-xylene, (c) ratio between disproportionation (yield of toluene) and isomerisation reaction (yield of p-xylene plus yield of o-xylene), (d) ratio between p-xylene and o-xylene yield in m-xylene isomerisation over Al-**UTL**, Al-IPC-7, Al-IPC-2 (ADOR mechanism preparation), Al-IPC-2 (one-pot synthesis), Al-IPC-6, Al-IPC-4 and ZSM-5-93 catalysts at WHSV 19 h^{-1} and 350 °C; ZSM-5-93 serves as benchmark.

The results of m-xylene isomerisation over Al-**UTL**, Al-IPC-n and ZSM-5-93 at the same WHSV 19 h^{-1} and temperature 350 °C are shown in Figure 4.14. Data calculated for samples taken after 5 min T-O-S were ambiguous, most probably because the system was still reaching a steady state, thus those points were neglected. The order of m-xylene conversions over ADOR catalysts is the same as in the reactions at WHSV 7.7 h^{-1}.

Al-IPC-2 one-pot showed the second highest conversion (53.7 % at 25 min T-O-S), as well as with acid site content (Figure 4.14 a, Table 4.3). The comparison of IPC-2 materials prepared by different approaches displays that, Al-IPC-2 one-pot shows higher conversion (53.7 % at 25 min T-O-S) than Al-IPC-2 ADOR (30.2 % at 25 min T-O-S). Al-IPC-2 ADOR was prepared using standard ADOR method, by the formation of S4Rs in between the layers of 2D precursor. Conversely, Al-IPC-2 one-pot was prepared from parent Al-**UTL**, by treatment in aluminium nitrate nonahydrate solution. This results in higher concentration of incorporated aluminium in this sample. Despite diverse synthetic processes, framework of Al-IPC-2 one-pot and Al-IPC-2 ADOR is the same, which was confirmed by PXRD and STEM imaging (Figure 4.5, Figure 4.6 and Figure 4.7). Also, textural properties of these catalysts are comparable (Table 4.1). The difference in aluminium content and therefore in acid sites content due to their synthetic process affects their catalytic performance. Aluminium content defines concentration of active sites and thus conversion (in case the acid sites are accessible) is higher. The Al-IPC-4 shows very low conversion (0.8 % at 25 min T-O-S) at WHSV of 19 h^{-1} (Figure 4.14 a) thus, it was not possible to evaluate the other parameters for this sample (Figure 4.14 b – d).

4.5.4   Summary of catalytic experiments

Yield of p-xylene, selectivity to p-xylene, ratio between the rate of disproportionation and isomerisation, and yield of p- to o-xylene are dependent on m-xylene conversion and therefore, for valid comparison of these parameters, they are shown as dependencies of conversion in Figure 4.15. In general, selectivity to p-xylene is increasing with decreasing conversion (Figure 4.15 b). Figure 4.15 c shows the ratio between bimolecular disproportionation and monomolecular isomerisation.

The presence of wider than 10-ring pores in the zeolite catalyst provides more space for bigger organic compounds and their transition states, therefore bimolecular disproportionation becomes more favoured reaction mechanism in 10-ring pores than in smaller pores (Figure 4.15 c). The narrowest channel of all studied catalysts is located at the intersection between the 10- and 8-ring channels system of Al-IPC-4. The least bulky among xylene molecules – p-xylene – diffuses through the pores of Al-IPC-4 easier than bigger o-xylene (Figure 4.15 d).

Figure 4.15 m-xylene conversion dependence of (a) yield of p-xylene, (b) selectivity to p-xylene, (c) ratio between disproportionation and isomerisation reaction, (d) ratio between p-xylene and o-xylene yield over Al-**UTL** (black), Al-IPC-7 (dark blue), Al-IPC-2 (ADOR mechanism preparation) (red), Al-IPC-2 (one-pot synthesis) (grey), Al-IPC-6 (green), Al-IPC-4 (orange), ZSM-5-93 (violet) catalysts at WHSV = 7.7 h^{-1} – 41 h^{-1}, and ZSM-5-59 (sky blue) at WHSV = 26 h^{-1} and 350 °C.

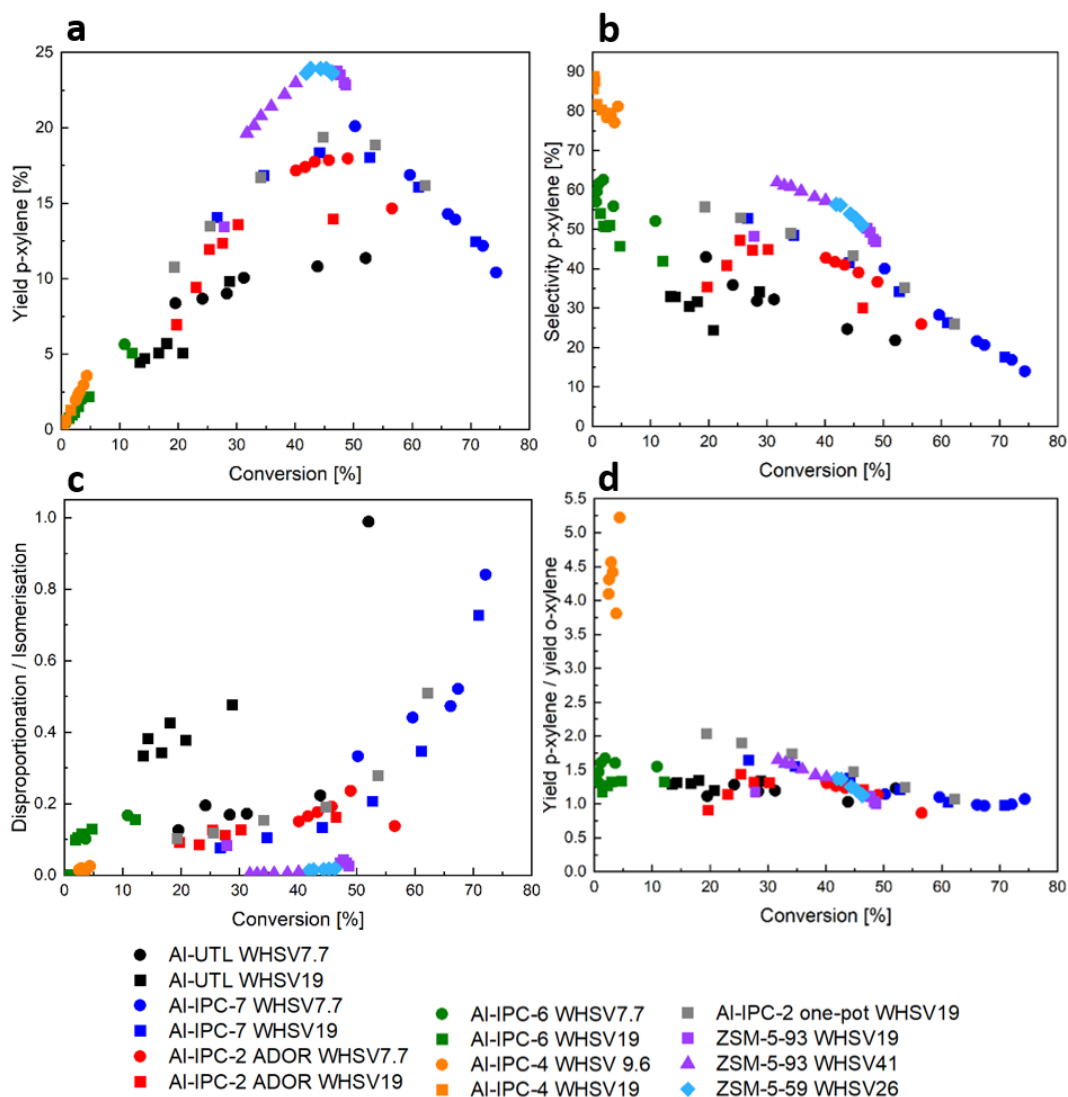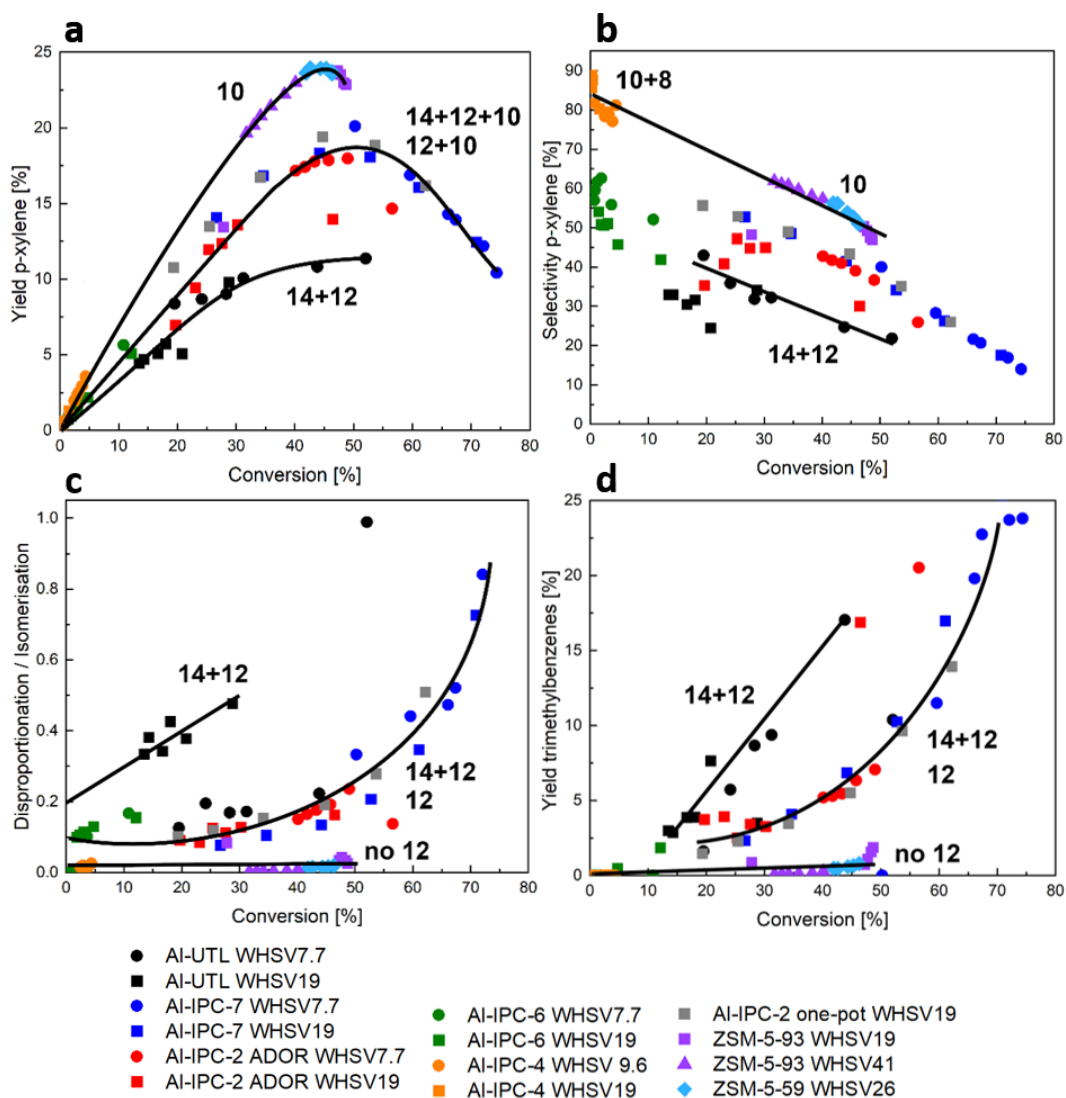**Figure 4.16** Highlighted observed trends in m-xylene conversion dependence of (a) yield of p-xylene, (b) selectivity to p-xylene, (c) ratio between disproportionation and isomerisation reaction, (d) yield of trimethylbenzenes over Al-**UTL** (black), Al-IPC-7 (dark blue), Al-IPC-2 (ADOR mechanism preparation) (red), Al-IPC-2 (one-pot synthesis) (grey), Al-IPC-6 (green), Al-IPC-4 (orange), ZSM-5-93 (violet) catalysts at WHSV = 7.7 h^{-1} – 41 h^{-1}, and ZSM-5-59 (sky blue) at WHSV = 26 h^{-1} and 350 °C. The numbers denote ring size of channel system in zeolite (*e.g.* 14+12 means 14-, 12-ring channel system).

For better clarification, observed trends in determined parameters (m-xylene conversion dependence of yield of p-xylene, selectivity to p-xylene, disproportionation to isomerisation ratio and yield of trimethylbenzenes) in m-xylene isomerisation reaction depending on pore sizes of utilised zeolites are shown in Figure 4.16. Pore sizes are decisive for the reaction selectivity. Zeolites with 8- and 10-ring pores (Al-IPC-4 and

ZSM-5) are the most selective (at low conversions) to p-xylene due to their smallest size of pore system (Figure 4.16 b) among studied ADOR zeolites. The 8-ring pores are not accessible for xylenes, therefore these channels behave like if they were not present. The 10-ring pores favour monomolecular isomerisation, as well as p-selectivity giving the highest yields of p-xylene due to suitable pore dimensions for diffusion of p-xylene molecules (Figure 4.16 a – c). Trimethylbenzenes are products of bimolecular reaction mechanism. Dependence of their yield on conversion exhibit qualitatively the same trends as disproportionation to isomerisation ratio parameter, confirming toluene is a well selected representative of the disproportionation reaction (Figure 4.16 d). Both, monomolecular isomerisation and bimolecular disproportionation, are enabled reaction mechanisms in zeolites with 12-ring channels and also in 14-ring channels (Figure 4.16 c). However, in 14-ring pores the large reaction space promotes also coke formation causing fast catalyst deactivation. Therefore, the fastest drop of m-xylene conversion occurs over Al-**UTL** with interconnected 14- and 12-ring channel system (Figure 4.13 a). Disproportionation to isomerisation ratio of almost 1 was observed in clean pores without coke prior to the catalyst deactivation. Catalyst performance is a combination of all the above contributions. It is important to mention, that previous studies of described isoreticular zeolites in liquid-phase tetrahydropyranylation showed that the catalytic behaviour of Al-IPC-7 does not correspond to a physical mixture of Al-**UTL** with Al-IPC-2, and Al-IPC-6 to a physical mixture of Al-IPC-2 with Al-IPC-4 [66]. We assume that the behaviour of these catalysts in isomerisation of m-xylene will be analogous, however this would require further studies to prove.

5   Conclusions

The aim of this work was to synthesise a set of isoreticular ADOR zeolites, characterise their properties, and investigate their shape selectivity in catalysed gas phase m-xylene isomerisation. Al-**UTL** zeolite was prepared *via* hydrothermal synthetic process. ADOR method was used for preparation of Al-IPC-7, Al-IPC-2, Al-IPC-6 and Al-IPC-4 from parent Al-**UTL**. Moreover, Al-IPC-2 zeolite was prepared by the 'one-pot' method to enhance the aluminium content in the final catalyst and compare its performance with 'standard' ADOR Al-IPC-2. All these materials are isoreticular, *i.e.* they possess the same crystalline layers, but the connections between layers are different. Therefore, those zeolites vary in the channel system. Synthesised materials were investigated in terms of structure, crystal morphology and texture, elemental content and acidity. Finally, catalysts were tested in m-xylene isomerisation.

Isomerisation of m-xylene was performed in the fixed-bed reactor using optimised reaction conditions: WHSV of 7.7 h^{-1} and 19 h^{-1}, at the temperature of 350 °C. Conversion of m-xylene over isoreticular zeolites increased in order: Al-IPC-4 < Al-IPC-6 < Al-**UTL** < Al-IPC-2 ADOR < Al-IPC-2 one-pot < Al-IPC-7. The catalyst performance was associated with the pore structure and acidity of the catalysts. The highest conversion was recorded for Al-IPC-7 zeolite that has interconnected 14- and 12-ring channels, along with 12- and 10-ring pore channels. Moreover, Al-IPC-7 sample had the highest concentration of acid sites. The one-pot synthetic strategy of Al-IPC-2 material resulted in higher amount of aluminium incorporated in the zeolite framework than standard stepwise preparation *via* layered precursor. The concentration of acid sites was higher in the Al-IPC-2 one-pot, which caused the higher conversions of m-xylene than Al-IPC-2 ADOR sample. Acid sites content was more important than pore structure for conversion determination over Al-**UTL**, Al-IPC-7 and Al-IPC-2 materials. The lowest conversions were observed for Al-IPC-6 and Al-IPC-4 catalysts due to prevalence of pore size effect over the acid sites content. The channel system of Al-IPC-4 zeolite (partially present in Al-IPC-6), consist of 8-ring channels that are inaccessible for organics, therefore these channels behave like they were not present. This caused a practical decrease of the channel dimensionality from 2D system (10-ring, 8-ring) to 1D system (only 10-rings accessible), it creates diffusion limitations, thus the observed conversion is relatively smaller than in case of catalysts with bigger pores (14-rings, 12-rings, and 10-rings present).

The two possible reaction pathways for m-xylene isomerisation reaction are monomolecular and bimolecular mechanisms. It was shown that generally zeolites with 10-ring channels favoured monomolecular isomerisation and provided high p-xylene selectivity. Bimolecular reaction mechanism was enabled in 12- and 14-ring channels. Additionally, the coke formation occurred in 14-ring channels which led to a relatively fast catalyst deactivation.

The presented results allow to understand the catalytic behaviour of investigated systems, however brought some open questions for further investigation. Follow up research should focus on the possible presence of extra-framework alumina species in the samples, especially those which were prepared in concentrated aluminium nitrate solutions and have interestingly high aluminium contents (Al-IPC-7, Al-IPC-2 one-pot). Possible methods to use for characterisation of this parameter can be ^{27}Al solid state NMR or XPS (X-ray photoelectron spectroscopy). Importantly, the characterisation of the spent catalysts should be performed to investigate their deactivation. Furthermore, we noticed the influence of two descriptors on the catalytic performance, thus the study of isoreticular catalysts with the same acidity, which would differ only in channel systems, would be beneficial. This would allow to study the exclusive effect of various pore system on m-xylene isomerisation.

References

[1]   C. Baerlocher, L.B. McCusker, D.H. Olson, *Atlas of Zeolite Framework Types*, 6th ed., Elsevier, 2007.

[2]   P. Eliášová, M. Opanasenko, P.S. Wheatley, M. Shamzhy, M. Mazur, P. Nachtigall, W.J. Roth, R.E. Morris, J. Čejka, The ADOR mechanism for the synthesis of new zeolites, *Chemical Society Reviews*. 44 (2015) 7177–7206.

[3]   P. Wheatley, P. Eliášová, H. Greer, W. Zhou, V. Seymour, D. Dawson, S. Ashbrook, A. Pinar, L. McCusker, M. Opanasenko, J. Čejka, R. Morris, Zeolites with Continuously Tuneable Porosity, *Angewandte Chemie International Edition*. 53 (2014) 13210–13214.

[4]   R. Millini, G. Bellussi, Zeolite Science and Perspectives, in: J. Čejka, R.E. Morris, P. Nachtigall (Eds.), *Zeolites in Catalysis: Properties and Applications*, The Royal Society of Chemistry, 2017: p. 1–36.

[5]   J. Yu, Synthesis of Zeolites, in: J. Čejka, H. van Bekkum, A. Corma, F. Schueth (Eds.), *Introduction to Zeolite Molecular Sieves*, 3rd ed., Elsevier, 2007: p. 39–104.

[6]   H.-K. Min, S.H. Cha, S.B. Hong, Mechanistic Insights into the Zeolite-Catalyzed Isomerization and Disproportionation of m-Xylene, *ACS Catalysis*. 2 (2012) 971–981.

[7]   C. Martínez, A. Corma, Inorganic molecular sieves: Preparation, modification and industrial application in catalytic processes, *Coordination Chemistry Reviews*. 255 (2011) 1558–1580.

[8]   S. Al-Khattaf, M.N. Akhtar, T. Odedairo, A. Aitani, N.M. Tukur, M. Kubů, Z. Musilová-Pavlačková, J. Čejka, Catalytic transformation of methyl benzenes over zeolite catalysts, *Applied Catalysis A: General*. 394 (2011) 176–190.

[9]   J. Čejka, B. Wichterlová, Acid-Catalyzed Synthesis of Mono- and Dialkyl Benzenes over Zeolites: Active Sites, Zeolite Topology, and Reaction Mechanisms, *Catalysis Reviews*. 44 (2002) 375–421.

[10]   S. Al-Khattaf, S.A. Ali, A.M. Aitani, N. Žilková, D. Kubička, J. Čejka, Recent Advances in Reactions of Alkylbenzenes Over Novel Zeolites: The Effects of Zeolite Structure and Morphology, *Catalysis Reviews*. 56 (2014) 333–402.

[11]   J. Weitkamp, M. Hunger, Acid and Base Catalysis in Zeolites, in: J. Čejka, H. van Bekkum, A. Corma, F. Schueth (Eds.), *Introduction to Zeolite Molecular Sieves*, 3rd ed., Elsevier, 2007: p. 787–836.

[12] C. Jo, R. Ryoo, N. Žilková, D. Vitvarová, J. Čejka, The effect of MFI zeolite lamellar and related mesostructures on toluene disproportionation and alkylation, *Catalysis Science & Technology*. 3 (2013) 2119–2129.

[13] W.J. Roth, P. Nachtigall, R.E. Morris, J. Čejka, Two-Dimensional Zeolites: Current Status and Perspectives, *Chemical Reviews*. 114 (2014) 4807–4837.

[14] K. Li, J. Valla, J. Garcia-Martinez, Realizing the commercial potential of hierarchical zeolites: New opportunities in catalytic cracking, *ChemCatChem*. 6 (2014) 46–66.

[15] C. Colella, Natural Zeolites and Environment, in: J. Čejka, H. van Bekkum, A. Corma, F. Schueth (Eds.), *Introduction to Zeolite Molecular Sieves*, 3rd ed., Elsevier, 2007: p. 999–1036.

[16] S. Mintova, J. Čejka, Micro/mesoporous Composites, in: J. Čejka, H. van Bekkum, A. Corma, F. Shueth (Eds.), *Introduction to Zeolite Molecular Sieves*, 3rd ed., Elsevier, 2007: p. 301–326.

[17] K.G. Strohmaier, Synthesis of Zeolites, in: J. Čejka, R.E. Morris, P. Nachtigall (Eds.), *Zeolites in Catalysis: Properties and Applications*, The Royal Society of Chemistry, 2017: p. 72–102.

[18] O. Shvets, N. Kasian, A. Zukal, J. Pinkas, J. Čejka, The Role of Template Structure and Synergism between Inorganic and Organic Structure Directing Agents in the Synthesis of UTL Zeolite, *Chemistry of Materials*. 22 (2010) 3482–3495.

[19] M. Shamzhy, O. Shvets, M. Opanasenko, P.S. Yaremov, L.G. Sarkisyan, P. Chlubná, A. Zukal, V.R. Marthala, M. Hartmann, J. Čejka, Synthesis of isomorphously substituted extra-large pore UTL zeolites, *Journal of Materials Chemistry*. 22 (2012) 15793–15803.

[20] L.B. McCusker, C. Baerlocher, Zeolite Structures, in: J. Čejka, H. van Bekkum, A. Corma, F. Schueth (Eds.), *Introduction to Zeolite Molecular Sieves*, 3rd ed., Elsevier, 2007: p. 13–38.

[21] T.F. Degnan, G.K. Chitnis, P.H. Schipper, History of ZSM-5 fluid catalytic cracking additive development at Mobil, *Microporous and Mesoporous Materials*. 35–36 (2000) 245–252.

[22] S. Smeets, X. Zhou, Zeolite Structures, in: J. Čejka, R.E. Morris, P. Nachtigall (Eds.), *Zeolites in Catalysis: Properties and Applications*, The Royal Society of Chemistry, 2017: p. 37–72.

[23] P. Sadeghpour, M. Haghighi, A. Ebrahimi, Ultrasound-assisted rapid hydrothermal design of efficient nanostructured MFI-Type aluminosilicate catalyst for methanol to propylene reaction, *Ultrasonics Sonochemistry*. 72 (2021) 105416.

[24] H. van Bekkum, H.W. Kouwenhoven, Progess in the Use of Zeolites in Organic Synthesis, in: J. Čejka, H. van Bekkum, A. Corma, F. Schuth (Eds.), *Introduction to Zeolite Molecular Sieves*, 3rd ed., Elsevier, 2007: p. 947–998.

[25] A. Julbe, Zeolite Membranes – Synthesis, Characterization and Application, in: J. Čejka, H. van Bekkum, A. Corma, F. Schueth (Eds.), *Introduction to Zeolite Molecular Sieves*, 3rd ed., Elsevier, 2007: p. 181–220.

[26] T. Bein, Host–Guest Interactions in Zeolites and Periodic Mesoporous Materials, in: J. Čejka, H. van Bekkum, A. Corma, F. Schueth (Eds.), *Introduction to Zeolite Molecular Sieves*, 3rd ed., Elsevier, 2007: p. 611–658.

[27] M. Mazur, J. Přech, J. Čejka, Zeolites and Other Micro- and Mesoporous Molecular Sieves, in: *Kirk-Othmer Encyclopedia of Chemical Technology*, Wiley Interscience, 2019: p. 1–36.

[28] W.J. Roth, P. Nachtigall, R.E. Morris, P.S. Wheatley, V.R. Seymour, S.E. Ashbrook, P. Chlubná, L. Grajciar, M. Položij, A. Zukal, O. Shvets, J. Čejka, A family of zeolites with controlled pore size prepared using a top-down method, *Nature Chemistry*. 5 (2013) 628–633.

[29] M. Mazur, P.S. Wheatley, M. Navarro, W.J. Roth, M. Položij, A. Mayoral, P. Eliášová, P. Nachtigall, J. Čejka, R.E. Morris, Synthesis of 'unfeasible' zeolites, *Nature Chemistry*. 8 (2016) 58–62.

[30] D.S. Firth, S.A. Morris, P.S. Wheatley, S.E. Russell, A.M.Z. Slawin, D.M. Dawson, A. Mayoral, M. Opanasenko, M. Položij, J. Čejka, P. Nachtigall, R.E. Morris, Assembly-Disassembly-Organization-Reassembly Synthesis of Zeolites Based on cfi-Type Layers, *Chemistry of Materials*. 29 (2017) 5605–5611.

[31] V. Kasneryk, M. Shamzhy, M. Opanasenko, P.S. Wheatley, S.A. Morris, S.E. Russell, A. Mayoral, M. Trachta, J. Čejka, R.E. Morris, Expansion of the ADOR Strategy for the Synthesis of Zeolites: The Synthesis of IPC-12 from Zeolite UOV, *Angewandte Chemie International Edition*. 56 (2017) 4324–4327.

[32] V. Kasneryk, M. Shamzhy, J. Zhou, Q. Yue, M. Mazur, A. Mayoral, Z. Luo, R.E. Morris, J. Čejka, M. Opanasenko, Vapour-phase-transport rearrangement technique for the synthesis of new zeolites, *Nature Communications*. 10 (2019) 5129.

[33] M. Trachta, O. Bludský, J. Čejka, R.E. Morris, P. Nachtigall, From Double-Four-Ring Germanosilicates to New Zeolites: In Silico Investigation, *ChemPhysChem*. 15 (2014) 2972–2976.

[34] E. Elderkamp, J. Gascon, F. Kapteijn, Zeolite Membranes in Catalysis, in: J. Čejka, R.E. Morris, P. Nachtigall (Eds.), *Zeolites in Catalysis: Properties and Applications*, The Royal Society of Chemistry, 2017: p. 481–518.

[35] M. Mazur, V. Kasneryk, J. Přech, F. Brivio, C. Ochoa-Hernández, A. Mayoral, M. Kubů, J. Čejka, Zeolite framework functionalisation by tuneable incorporation of various metals into the IPC-2 zeolite, *Inorganic Chemistry Frontiers*. 5 (2018) 2746–2755.

[36] M. Mazur, M. Kubů, P.S. Wheatley, P. Eliášová, Germanosilicate UTL and its rich chemistry of solid-state transformations towards IPC-2 (OKO) zeolite, *Catalysis Today*. 243 (2015) 23–31.

[37] N. Žilková, P. Eliášová, S. Al-Khattaf, R.E. Morris, M. Mazur, J. Čejka, The effect of UTL layer connectivity in isoreticular zeolites on the catalytic performance in toluene alkylation, *Catalysis Today*. 277 (2016) 55–60.

[38] W. Vermeiren, J.-P. Gilson, Impact of Zeolites on the Petroleum and Petrochemical Industry, *Topics in Catalysis*. 52 (2009) 1131–1161.

[39] S.F. Abdo, S.T. Wilson, Zeolites in Industrial Catalysis, in: J. Čejka, R.E. Morris, P. Nachtigall (Eds.), *Zeolites in Catalysis: Properties and Applications*, The Royal Society of Chemistry, 2017: p. 310–350.

[40] K. Tanabe, W.F. Hölderich, Industrial application of solid acid–base catalysts, *Applied Catalysis A: General*. 181 (1999) 399–434.

[41] A.J. Jones, R.T. Carr, S.I. Zones, E. Iglesia, Acid strength and solvation in catalysis by MFI zeolites and effects of the identity, concentration and location of framework heteroatoms, *Journal of Catalysis*. 312 (2014) 58–68.

[42] S. Bordiga, C. Lamberti, F. Bonino, A. Travert, F. Thibault-Starzyk, Probing zeolites by vibrational spectroscopies, *Chemical Society Reviews*. 44 (2015) 7262–7341.

[43] S. Mohan, P. Dinesha, S. Kumar, NOx reduction behaviour in copper zeolite catalysts for ammonia SCR systems: A review, *Chemical Engineering Journal*. 384 (2020) 123253.

[44] T.F. Degnan, Applications of zeolites in petroleum refining, *Topics in Catalysis*. 13 (2000) 349–356.

[45] M. Guisnet, N.S. Gnep, S. Morin, Mechanisms of xylene isomerization over acidic solid catalysts, *Microporous and Mesoporous Materials*. 35–36 (2000) 47–59.

[46] B. Adair, C.-Y. Chen, K.-T. Wan, M.E. Davis, Reactions of meta-xylene on zeolites with intersecting medium and large pores I. Basic studies, *Microporous Materials*. 7 (1996) 261–270.

[47] R.E. Morris, P.K. Allan, Structure Determination, in: J. Čejka, R.E. Morris, P. Nachtigall (Eds.), *Zeolites in Catalysis: Properties and Applications*, The Royal Society of Chemistry, 2017: p. 194–239.

[48]   R.E. Morris, P.S. Wheatley, Diffraction Techniques Applied to Zeolites, in: J. Čejka, H. van Bekkum, A. Corma, F. Schueth (Eds.), *Introduction to Zeolite Molecular Sieves*, 3rd ed., Elsevier, 2007: p. 375–402.

[49]   D.N. Rainer, M. Mazur, Electron microscopy methods for characterisation of zeolite catalysts, in: *Catalysis: Volume 32*, The Royal Society of Chemistry, 2020: p. 151–187.

[50]   K.A. Cychosz, M. Thommes, Progress in the Physisorption Characterization of Nanoporous Gas Storage Materials, *Engineering*. 4 (2018) 559–566.

[51]   J. Rouquerol, F. Rouquerol, P. Llewellyn, G. Maurin, K. Sing, *Adsorption by Powders and Porous Solids: Principles, Methodology an Applications*, Academic Press, 2014.

[52]   S. Lowell, J.E. Shields, M.A. Thomas, M. Thommes, *Characterization of Porous Solids and Powders: Surface Area, Pore Size and Density*, Springer, 2004.

[53]   E.P. Barrett, L.G. Joyner, P.P. Halenda, The Determination of Pore Volume and Area Distributions in Porous Substances. I. Computations from Nitrogen Isotherms, *Journal of the American Chemical Society*. 73 (1951) 373–380.

[54]   M. Thommes, K.A. Cychosz, Physical adsorption characterization of nanoporous materials: Progress and challenges, *Adsorption*. 20 (2014) 233–250.

[55]   A. Bazilio, J. Weinrich, The Easy Guide to: Inductively Coupled Plasma-Mass Spectrometry (ICP-MS), 2012.

[56]   A. Lebedev, General Principles of Mass Spectrometry, in: A. Lebedev (Ed.), *Comprehensive Environmental Mass Spectrometry*, ILM Publications, 2012: p. 1–20.

[57]   S.F. Anis, A. Khalil, Saepurahman, G. Singaravel, R. Hashaikeh, A review on the fabrication of zeolite and mesoporous inorganic nanofibers formation for catalytic applications, *Microporous and Mesoporous Materials*. 236 (2016) 176–192.

[58]   J.A. Lercher, A. Jentys, Infrared and Raman Spectroscopy for Characterizing Zeolites, in: J. Čejka, H. van Bekkum, A. Corma, F. Schueth (Eds.), *Introduction to Zeolite Molecular Sieves*, 3rd ed., Elsevier, 2007: p. 435–476.

[59]   B. Wichterlová, Z. Tvarůžková, Z. Sobalík, P. Sarv, Determination and properties of acid sites in H-ferrierite: A comparison of ferrierite and MFI structures, *Microporous and Mesoporous Materials*. 24 (1998) 223–233.

[60]   H. Günther, Introduction, in: *NMR Spectroscopy: Basic Principles, Concepts and Applications in Chemistry*, 3rd ed., Wiley-VCH, 2013: p. 1–7.

[61] F.G. Kitson, B.S. Larsen, C.N. McEwen, What is GC/MS?, in: *Gas Chromatography and Mass Spectrometry : A Practical Guide*, Academic Press, 1996: p. 3–23.

[62] F.L. Dorman, P. Dawes, Column Technology: Open Tubular Column, in: *Gas Chromatography*, Elsevier, 2012: p. 79–96.

[63] M.S. Klee, Detectors, in: *Gas Chromatography*, Elsevier, 2012: p. 307–348.

[64] B.C. Lippens, J.H. de Boer, Studies on pore systems in catalysts: V. The t method, *Journal of Catalysis*. 4 (1965) 319–323.

[65] R. Giudici, H.W. Kouwenhoven, R. Prins, Comparison of nitric and oxalic acid in the dealumination of mordenite, *Applied Catalysis A-General*. 203 (2000) 101–110.

[66] Y. Zhou, S. A. Kadam, M. Shamzhy, J. Čejka, M. Opanasenko, Isoreticular UTL-Derived Zeolites as Model Materials for Probing Pore Size–Activity Relationship, *ACS Catalysis*. 9 (2019) 5136–5146.